Summer 2010

Implementing frequency regulation capability in a solar photovoltaic power plant

Venkata Ajay Kumar Pappu

Department:

IMPLEMENTING FREQUENCY REGULATION CAPABILITY IN A SOLAR PHOTOVOLTAIC POWER PLANT

by

VENKATA AJAY KUMAR PAPPU

A THESIS

Presented to the Faculty of the Graduate School of the

MISSOURI UNIVERSITY OF SCIENCE AND TECHNOLOGY

In Partial Fulfillment of the Requirements for the Degree

MASTER OF SCIENCE IN ELECTRICAL ENGINEERING

2010

Approved by

Badrul H. Chowdhury, Advisor
Mariesa L. Crow
Mehdi Ferdowsi

ABSTRACT

Photovoltaic power plants pose some challenges when integrated with the power grid. Today's PV plants focus on extracting the maximum power from the arrays. This makes the PV system unavailable for helping in regulating the grid frequency as compared to conventional synchronous generators. A new technique for tracking a pseudo-maximum power point for creating power reserve is presented. This will help provide fast response in injecting power to respond to rapid load changes in a manner analogous to the inertia of a rotating machine. This helps in contributing toward frequency regulation.

This thesis examines the implementation of a two stage power conversion model in Simulink/Matlab that uses the reserve power algorithm. A GE-PV 200W solar panel has been used to simulate a 2 kW system. The new technique is discussed in detail and simulation results are provided.

ACKNOWLEDGMENTS

I owe my deepest gratitude to my advisor Dr. Badrul Chowdhury, for his never ending support and encouragement at all times. I am grateful to him for providing me with financial support. He has always been a great source of motivation and guided me through many important aspects of my graduate career. I am indebted to him for everything he has done for me from the beginning of my Masters program. I would like to thank Intelligent Systems Center for funding this project and making me a part of it.

I would like to thank Dr. Mariesa Crow and Dr. Mehdi Ferdowsi, Department of Electrical and Computer Engineering for serving on my committee, taking their valuable time to review my thesis and being great course instructors.

I would like to thank Dr. Jonathan Kimball for his support during my research. I would like to thank Luke Watson and Ravi Bhatt, my friends and project partners for their contribution to a good research group.

I would like to thank Regina Kohout, secretary for electrical and computer engineering department for being a constant well wisher and helping me at all times.

It is a pleasure to thank all those who made my stay in Rolla memorable: Uday Rao, Manoj Tirumalasetty, Vennela Yadhati, Mehul Madan, Shweta Neglur, Anand Prabhala, Murali Mohan Baggu, Fanjun Meng, Hengsi Qin, Theresa and Xiaomeng Li.

I would like to thank my father, Ashok Pappu; my mother, Jayasri; my late grandfather Prakasa Rao and my brother Vijay Pappu and for encouraging me to pursue my Master's degree and their constant love and support throughout my study program.

TABLE OF CONTENTS

LIST OF ILLUSTRATIONS

LIST OF TABLES

1. INTRODUCTION

1.1 BACKGROUND

An ever increasing demand for energy and environmental concerns in the 21st century has led to a sustained effort to generate power from various alternative energy resources. Although coal and hydro power plants are still used to produce electric power on a large scale, renewable energy has been of primary focus in recent years due to their abundance. With issues such as global warming and depletion of fossil fuels, generation from alternate energy resources such as wind and solar power has been increasing steadily. The rate at which photovoltaic (PV) power generation is projected to increase by 2030 is promising in many aspects. Figure 1.1 illustrates the projected growth of PV systems capacity through the year 2030 [1].

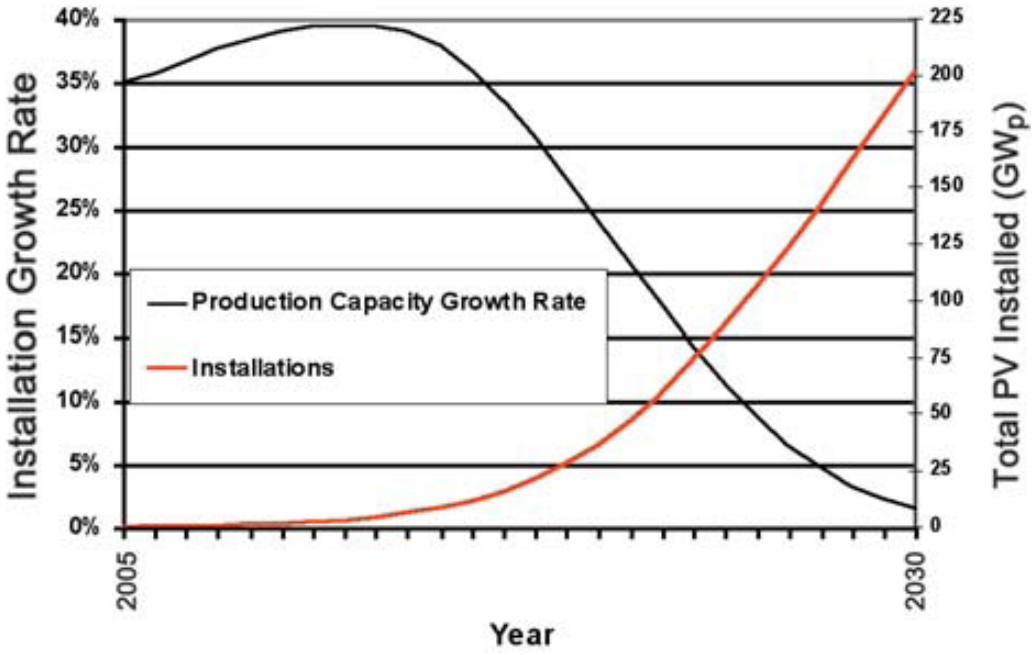

Fig. 1.1: Increase in PV generation capacity by 2030.

PV generation has increased on a large scale especially in the US and Europe, with one of the largest plants rated at 60MW at Olmedilla, Spain [2]. It has become necessary to understand how the power system will behave under the integration of such huge intermittent generating plants and their proper usage at the distribution level in Microgrids.

A microgrid is typically built around a low-voltage (LV) distribution systems with distributed energy resources (DERs) such as micro-turbines, fuel-cells, PV arrays, etc. [3-5]. Photovoltaic systems form an important part of a renewable energy generation portfolio since they are pollution free when operating, are modular in nature which makes construction easier, and they have relatively long life.

1.2 OBJECTIVE

In a typical grid-tied operating mode, PV systems are made to operate at the maximum power point by actively tracking the array voltage and current at all times. This will ensure that the maximum possible power is generated from the arrays for a given insolation. Figure 1.2 shows the general characteristic curve of a PV array and how it varies with voltage.

In an energy-limited system, such as a microgrid, this mode of operation is not helpful as the PV system is generally not able to follow the load demand or participate in frequency regulation. In addition, in the special case when the microgrid is comprised of many other DERs that are renewable in nature, load following will become a critical function needed to maintain the frequency and voltage of the microgrid [6]. An example of this type of microgrid is a forward operating military base. Since the system frequency

and voltage are generally decoupled, mainly deviating from their nominal values because of the imbalances in the active power and reactive power, respectively, the design of the control and optimization methodology becomes quite complex and challenging.

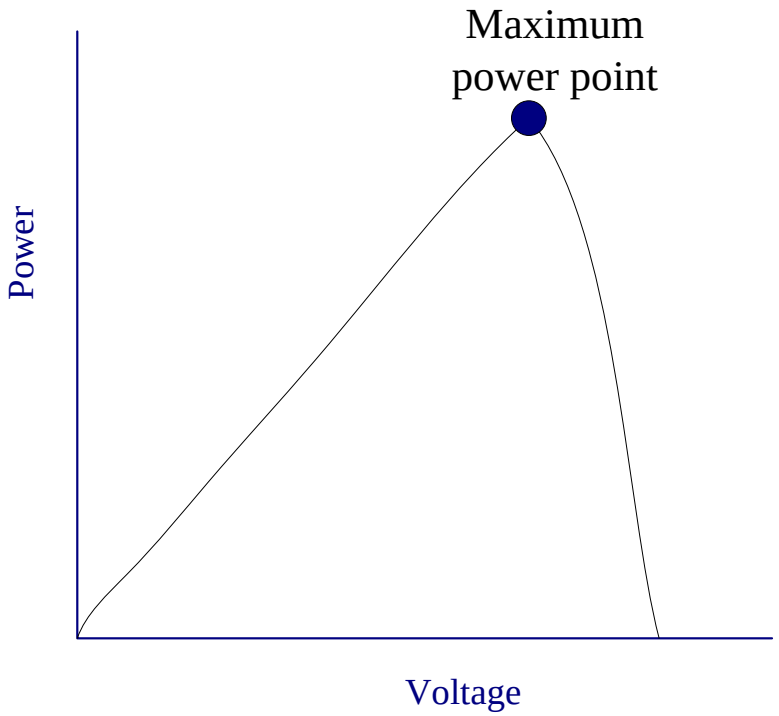

Fig. 1.2: Power-voltage characteristics of a solar panel.

A single or two stage conversion topology may be implemented to extract power from the PV array. A single stage system will have the maximum power point tracker (MPPT) integrated into the inverter control that will convert the dc power from the array into ac power. A system can be designed with two different loops: one for the pulse width modulation (PWM) control of the inverter and another for the MPPT that determines the power output [7]. However such designs which use only a single stage inverter from the

PV array do not have a provision to integrate additional elements such as energy storage that requires a constant dc bus voltage. It also has a drawback that complex controls need to be implemented for extracting the power and converting it into ac.

In this thesis, a two-stage power conversion consisting of a dc-dc boost converter and a single phase inverter with feedback control is used for the implementation of frequency regulation control [8]. The dc-dc converter is driven by a modified maximum power point tracker for the PV array. The modified MPPT algorithm will enable the system to go into a 'reserve power' mode when necessary. The reserve power calculation is built into the MPPT algorithm.

The purpose of the MPPT algorithm is to extract the maximum available power from the array. In this thesis, an alternate approach of tracking a pseudo-MPP has been implemented in order to have more control over the active power that can be injected into the grid. Although any type of PV cell will work, for the purpose at hand, a particular model of the polycrystalline solar cell is adopted. The grid connection of the solar modules has to guarantee maintenance of stability when the microgrid operates in an islanded condition. The reserve power from the array can be used to ride through the intermittency of the resource and help in system frequency regulation.

Whenever there is a drop in frequency of the system below a certain level or increase above a certain level, it is compensated, at least partially, by increasing or decreasing the power generation from the PV system, respectively, similar to a governor action in a conventional generator.

For the analysis of the system, the MPPT and the array model have been simulated using Matlab/Simulink version R2008b while the dc-dc converter and the single phase inverter have been designed using PLECS version 3.0.2.

1.3. THESIS FORMAT

The thesis is divided into various sections and described in detail as follows. The generation of solar power and the various types of solar cells that are used are described in Section 2. It describes the temperature dependence on different solar cells along with a description of recent trends in solar cell technology. The photovoltaic panel and its modeling in detail and its characteristics graphs at various temperatures and insolation are shown in Section 4.

The modified MPPT algorithm used for the purpose of getting the reserve power in the system obtained by the combination of two MPPT algorithms are discussed in Section 5. Section 6 gives the description of the dc-dc boost converter and the single phase inverter modeling and design considerations. The simulations and test results on the system for different cases and related analysis of how the reserve power in the PV system is implemented are shown separately in Section 7. Section 8 contains the conclusions inferred from the simulation study and analysis.

2. SOLAR POWER GENERATION IN POWER SYSTEM

2.1 SOLAR POWER GENERATION

Power generation from many renewable sources is not always constant; it varies with time and weather conditions and is therefore inherently intermittent. Solar power is no exception and the variation in solar power is due to the varying insolation at different times of the day and also affected by cloud cover and ambient temperature. Because of this variation of the output power, systems have been developed to tap the complete potential of the PV plant. Generation of solar power at the microgrid level is being done on a large scale due to many benefits such as reduction in costs of transmission, safe long term and reliable power supply [9].

2.2 TYPES OF SOLAR CELLS

2.2.1 Introduction. The different types of solar cells are discussed in the following sections. The cells have been compared keeping in mind the variation or changes in characteristics with temperature, voltage and irradiance.

2.2.2 Amorphous Solar Cells. Amorphous solar cells are made by depositing a thin film of silicon onto a sheet of another material such as steel. The panel is formed as one piece and the individual cells are not as visible as in other types.

Their advantage lies in their relatively low cost per Watt of power generated. However, this is offset by their lower power density as more panels are needed for the same power output and therefore more space is taken up. [10]

However, these cells have drawbacks in that their output impedance is high so that when more current is drawn from the cells, it results in reduction of the voltage.

2.2.3 Crystalline Solar Cells. Crystalline solar cells are wired in series to produce solar panels. As each cell produces a voltage of between 0.5 and 0.6 Volts, so a large number of cells need to be connected in series to produce an open-circuit voltage of the required value. Although the theoretical efficiency of monocrystalline cells is slightly higher than that of polycrystalline cells, there is little practical difference in performance. Crystalline cells generally have a longer lifetime than the amorphous variety [11].

2.2.4 Thin Film Solar Cells. These cells have the potential to reduce material costs as it uses very thin films on low cost substrate such as glass, stainless steel etc. The most widely used type is the silicon based thin film solar cell: amorphous (a-Si:H) and micro crystalline (µc-Si:H) single junction and tandem. These cells have no stability problems even though they have almost the same band gap energy as the crystalline Si cells. The major difference between these two types comes from the electro-optical properties of intrinsic Si-films that absorb the photons from sunlight.The a-Si:H film has a bandgap of 1.7-1.8eV. Solar cells having this material normally give high voltage and low current.

With the introduction of a-Si:H in the 1970's, more than 25% of the market share was owned by these models, but reduced drastically later on because of the low efficiency and stability problem. µc-Si:H solar cells have both crystalline and amorphous Si plus grain boundaries. They have the same band gap energy, but the efficiency is about 10% only [12]. Usually, a combination of both the amorphous and microcrystalline cells is used. The higher photon energy is absorbed by a-Si:H and low energy by the µc-Si:H. Higher voltages can be achieved by a series connection of the two cells and is useful in reducing the series resistance loss.

2.2.5 Solar Cells With Efficiency Greater Than 20%. A new generation of high efficiency crystalline solar cells based on the Obliquely Evaporated Contact (OECO) technology was introduced in the year 2000. These cells have a superior performance from -40 C to 80 C. For the standard size of 10 x 10 cm^2 efficiencies up to 20 % was achieved.

85% of the present PV installations are made from wafer based crystalline silicon solar cells. The Plasma enhanced chemical vapor deposition (PECVD) of SiN technology is used for the design of these cells [13].

2.3 EFFECT OF TEMPERATURE ON I-V CURVES FOR SOLAR CELLS

The performance of the solar cells is affected by the temperature and solar irradiance.

The dependency on temperature is checked based upon interpolation techniques. The output voltage V is a linear function of temperature T when output current is constant and is given by:

$$I_3V = I_1(V) + \frac{E_3 - E_1}{E_2 - E_1}.(I_2(V) - I_1(V)) \tag{2.1}$$

$$V_3(I) = V_1(I) + \frac{T_3 - T_1}{T_2 - T_1}.(V_2(I) - V_1(I)) \tag{2.2}$$

The subscripts indicate measured conditions and target conditions on the I-V curves for 3 different points 1, 2 and 3 (target point). Two important things are assumed while analyzing the dependence [14]:

- The current has two parts, a dark current and voltage dependent photo-current that is directly proportional to the irradiance of short circuit current.
- Output voltage is a function of temperature T when output current is constant.

Based on the results given by Yuki and Kosuke [14], the variation in I-V curves for crystalline and amorphous solar cells is as illustrated in Figs. 2.1 and 2.2, respectively.

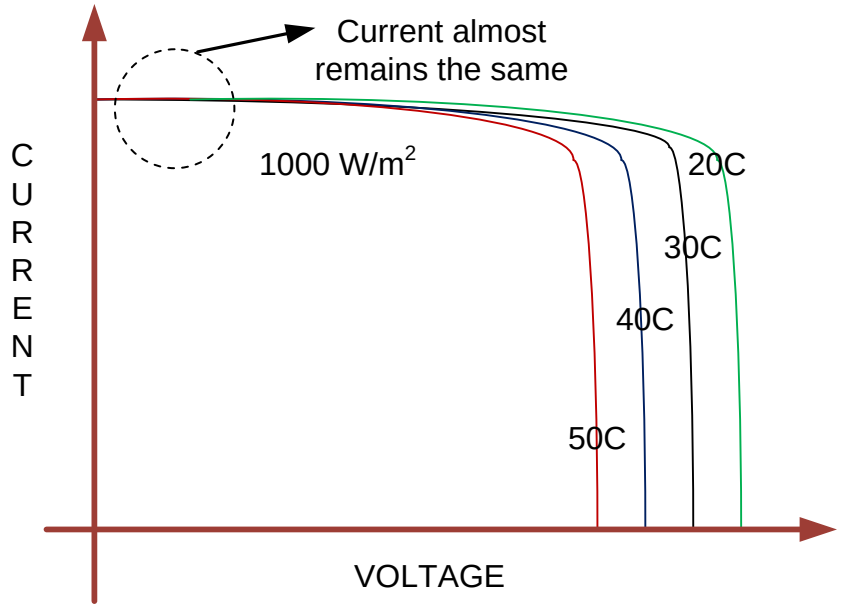

Fig. 2.1: Variation in the I-V curve for crystalline solar cell with temperature.

As shown in Fig. 2.1, the current remains almost constant for variations in temperature for the solar cell, whereas for an amorphous solar cell for the same variation in temperature, the voltage values are more constrained as observed in Fig. 2.2.

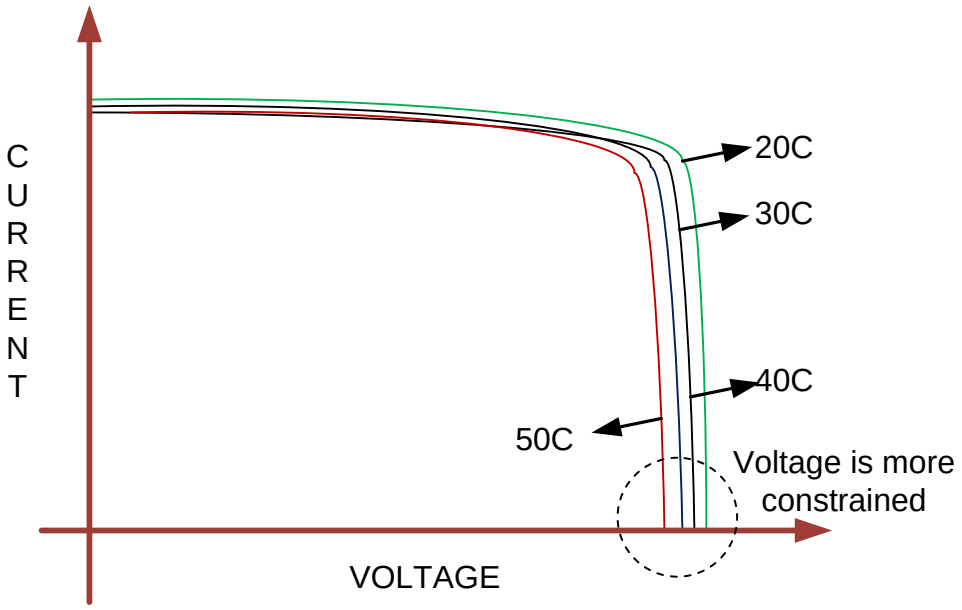

Fig. 2.2: Variation in the I-V curve for amorphous solar cell with temperature.

The temperature dependence plays a key role in the performance of a solar cell based on its application. If the usage involves a power conversion stage, then the rapid variation in the cell voltage should have to be controlled by an effective MPPT controller. The comparison of the variation in the voltage values for the solar cells suggests that an amorphous solar cell will perform better even under large variation of voltage values. But since the cost factor of the crystalline solar cells is really low as shown in Table 2.1, they are mostly used for large scale applications.

A complete analysis and comparison of various types of solar cells described in this section are presented in Table 2.1.

Table 2.1: Comparison of different kinds of solar cells

Performance factor\Type of cell	Crystalline	a-Si & µCryst tandem cells	Cells with efficiency > 20 %	Thin film Si:H cells (Amorphous)
Cell structure	Simple layer of crystalline Si form	Dual layered with varying thickness of both amorphous and crystalline.	Simple layer but different conc of many doping materials	Proto crystalline thin film
Efficiency	Around 10%	Between 13-15% under various thickness values	>20% under normal conditions & between 18-20 under higher temperatures	>10%
Synthesis process	Screen printing	Multi chamber PECVD & VHFCVD[12]	OECO technique[13]	Hydrogen dilution & protocrystallinity
Cost factor	Inexpensive	Inexpensive (sometimes less than crystalline)	Low cost for large scale production	Costly
Commercial Availability	Good but decreasing	On the rise in the past decade	Not available commercially	Under production by many solar companies
Effect of temperature	Current is Constant	Bigger range of output voltage	Almost similar to crystalline	Output voltage at lower values

The production of some special solar cells requires complex techniques like the ones that have a high efficiency as shown in Table 2.1. Until the application of such techniques is widely used in industry using polycrystalline or amorphous solar cells will

reduce cost for large scale PV installations. The comparison has been made on some key features such as structure, efficiency, synthesis process, availability and temperature.

A polycrystalline solar array has been selected for the system in the thesis and the response under varying conditions of temperature and insolation has been shown.

3. SYSTEM DESCRIPTION

3.1 SYSTEM OVERVIEW

The full system is implemented in a two stage power conversion which is connected to the grid on the inverter side. The different stages of the system are illustrated in Fig. 3.1 with two independent control loops for the dc-dc converter and the single phase dc-ac inverter.

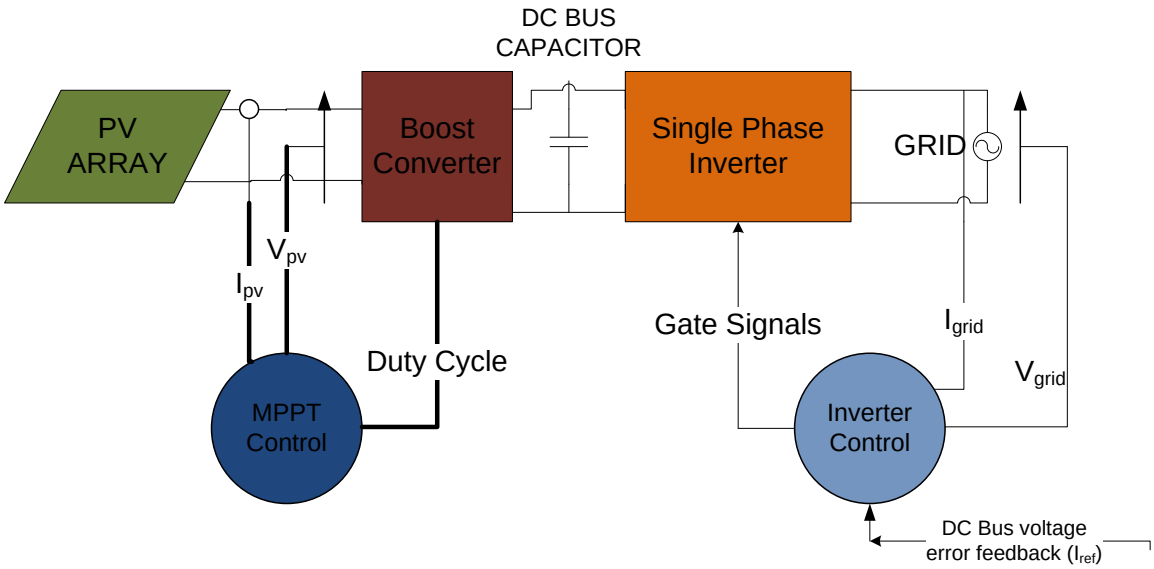

Fig. 3.1: Topology of the implemented system.

For the simulation in the thesis, a GE-PV 200W solar panel has been used to build a 2 kW PV array. A boost converter with a single phase inverter which steps up the voltage to the grid level of 340Vp-p has been simulated along with the PV array in a two

stage power conversion system. The key advantage with a two stage system is that the grid voltage can be varied over a wide range and eliminates the need for customization of the PV system for various utility applications [15]. This is very important for microgrids where there are certain operational requirements.

A two stage power conversion system also enables one to have an effective control over the power transfer with two independent control loops, i.e., one on the dc side and the other on the ac side. This thesis concentrates on effective control of active power that is injected into the system, and it is for this reason that a two stage conversion scheme has been used as this gives more flexibility over the control.

The MPPT control loop works based on the PV voltage and current inputs. The inverter control loop has inputs of grid voltage, grid current along with the dc bus voltage error feedback.

3.2 NEED FOR ACTIVE POWER CONTROL IN THE PV SYSTEM

Photovoltaic systems are made to work under their maximum power generating conditions by the MPPT. They always track the maximum available power under various insolation values. Because of this constraint, they find limited application in load following and frequency regulation.

For a stable and reliable operation of a power system the frequency needs to be maintained constant at 60 Hz. This is done by maintaining a balance between the active power generated and consumed in the system. Large scale PV systems in the range of 50MW-60MW are now being built and integrated into the power system. When such

large PV systems are connected, their participation in the frequency control and load following becomes essential for reliable operation of the grid.

To achieve this functionality, effective control over the active power of the PV plant is important. In conventional generators, the action of the prime mover allows the system to gain control over frequency [16].

Such a methodology is absent in PV plants and therefore has to be developed. Figure 3.2 shows the droop line control of a controllable power plant. For a change in frequency from f_1 to f_2 there is a corresponding increase in prime mover power from P_1 to P_2 [17]. This control is absent in a PV power plant since the focus is on obtaining the maximum available power from the solar insolation at a particular instant.

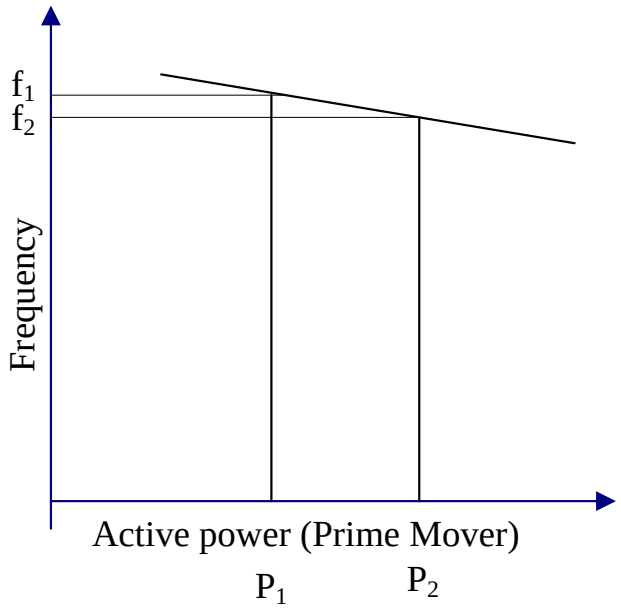

Fig. 3.2: Droop line of a controllable power plant.

In this thesis, this control over the active power of the PV plant has been developed. This enables load follow capability along with the frequency regulation in a micro-grid.

Making the PV systems generate variable amounts of power for a given insolation has many advantages as explained above. In a micro-grid when several renewable sources work together with the proposed control, then the voltage and frequency management is possible even under islanded operating conditions.

4. PHOTOVOLTAIC ARRAY

4.1 PV ARRAY PERFORMANCE

The general circuit model of a photovoltaic cell is shown in Fig. 4.1.

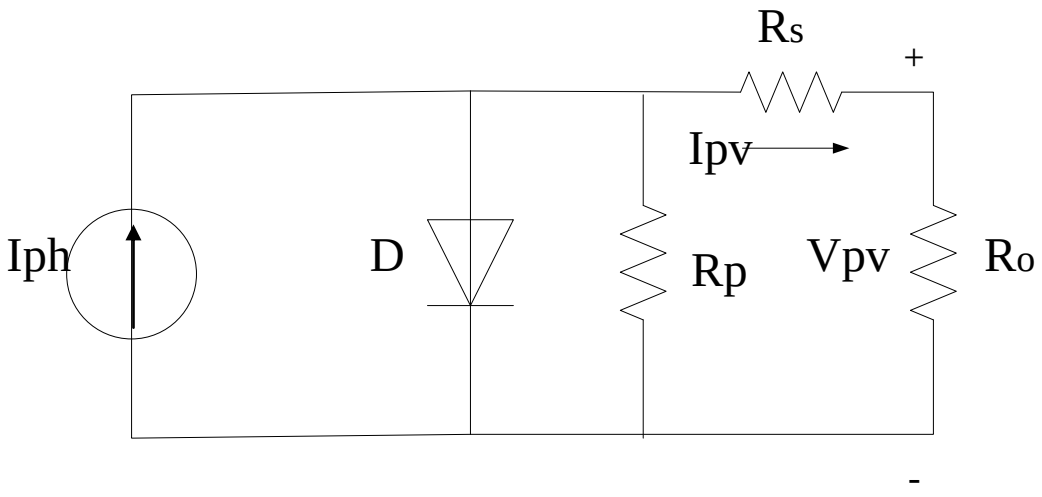

Fig. 4.1: Solar cell circuit model.

The governing equation is given by (4.1):

$$I_{pv} = I_{ph} - I_o(\exp((V_{pv} + I_{pv} * R_s) / A * V_t) - 1) - (V_{pv} + I_{pv} * R_s) / R_p \quad (4.1)$$

Where,

I_{pv} -- PV cell current

V_{pv} -- PV cell voltage

I_{ph} - Photocurrent of the diode

I_o - saturation current of the diode

R_s – Series resistance of the cell

R_p – Parallel resistance of the cell

The solar cell when exposed to sun's irradiation will generate dc power. The amount of dc power generated is directly dependent on the intensity of the solar irradiance. The characteristics of the diode are responsible for the behavior of the solar cell such that for short circuit and open circuit of the solar cell the current will either flow or get blocked, respectively [18]. The model used here consists of one diode in the cell circuit.

Since the relationship between the solar panel's voltage and current is not linear and varies with insolation and temperature, a maximum power point tracker is needed for the extraction of maximum possible power. This system is similar to the stand alone PV systems discussed in [19] but does not have a battery storage integrated into it. The PV array is to be integrated with power converters for effective control and transfer of power from the array to the grid or load side. This is done using a dc-dc converter along with a dc-ac inverter. The maximum power tracking control scheme is implemented as a control block for switching the converter to extract the maximum power.

The open source PV array model developed by the University of Colorado [20] has been used as a reference to develop this temperature dependent solar array in Matlab/Simulink. The model is dependent on temperature and insolation (E) to which the array is exposed. An overview of the model is shown in Fig. 4.2.

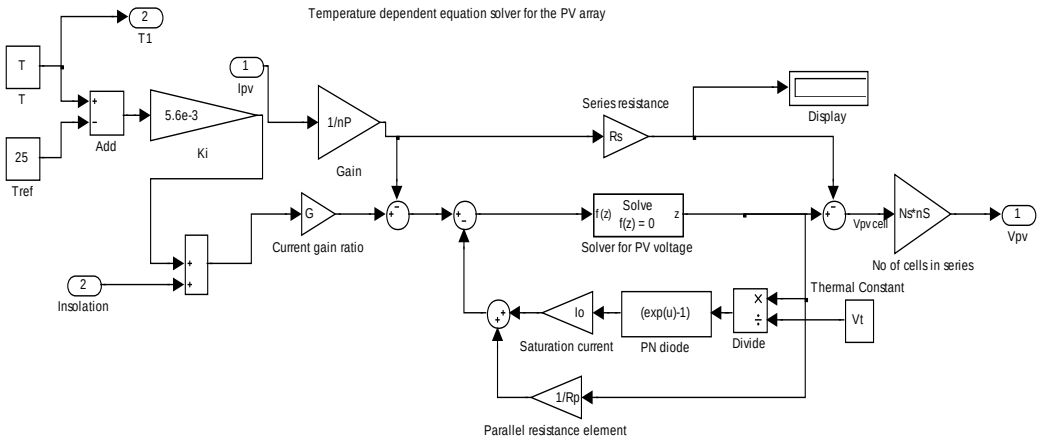

Fig. 4.2: Simulink model of the solar cell.

Some models as the one proposed by Altas [21] uses correction factors methodology for developing the solar array model for different temperatures. While this method develops different constants for the module, a similar technique has been used in the development of this PV block in this thesis. But the parameters from the solar array data sheet have been used in the temperature dependent equations for the panel as explained in Section 4.2.

This cell model is modified to simulate a 2 kW PV system with different array configurations nP representing the number of strings of arrays in parallel and nS is the number of arrays in a single string. PV system of this capacity has been used in the final system integrated with the converters to inject power into the grid. These parameters should have to be entered into the PV system block before simulation For the system

under consideration, to get a 2 kW output, 2 parallel strings with 5 panels in each string has been used to generate a voltage of (26.3*nS = 131.5V) and a maximum power point current of (7.6*nP = 15.2A). The 2 kW system equivalent is shown in Fig. 4.3. For the system used nS = 5 and nP = 2.

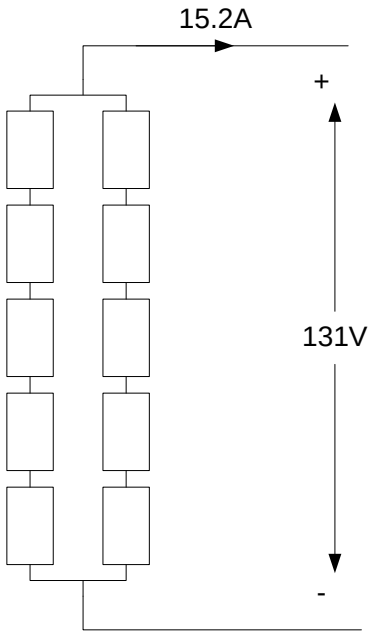

Fig. 4.3: 2 kW PV system arrangement.

4.2. TEMPERATURE DEPENDENCE

The parameters from the GE PV solar panel data sheet have been used in implementing the temperature dependent equations. The constants used from the solar panel data sheet are short circuit temperature coefficient (K_i) = 5.6 mA/^{o}C, open circuit

voltage coefficient (K_v) = -0.12 V/^oC. This GE solar panel has 54 polycrystalline cells connected in series. The following equations show the variation of parameters with temperature.

The dependence of photo current on temperature is given by (4.2) [22]:

$$I_{ph} = (E + (T - 25)K_i) \times I_{sc} / 1000 \tag{4.2}$$

Where I_{sc} is the short circuit current and T the temperature in degree centigrade and the nominal temperature is 25^oC. The open circuit voltage is given by (4.3)

$$V_{oc}' = [V_{oc} + (K_v \times (T - 25))] \tag{4.3}$$

Where V_{oc} is the open circuit voltage at nominal temperature and K_v is the voltage coefficient. Figures 4.4 and 4.5 show the variation in output current of the solar array with insolation and temperature, respectively.

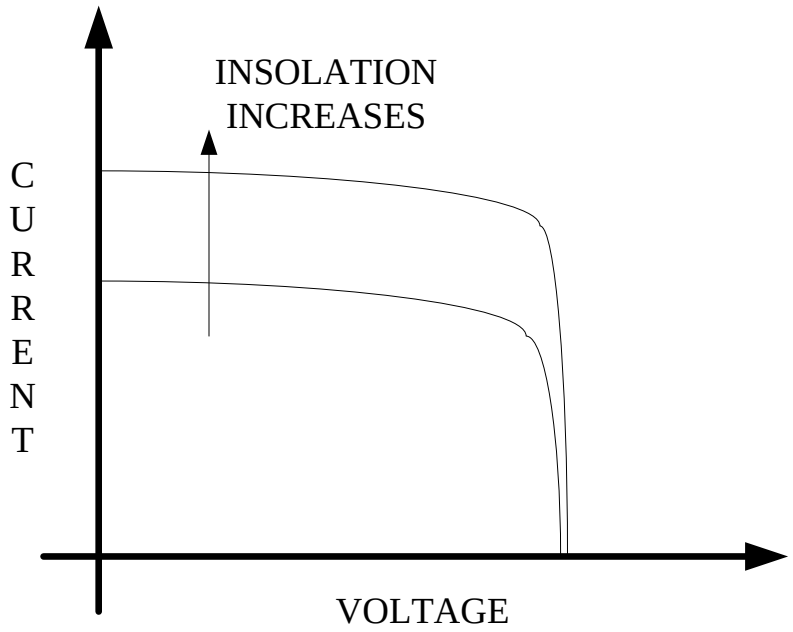

Fig. 4.4: Change in the short circuit current with varying insolation.

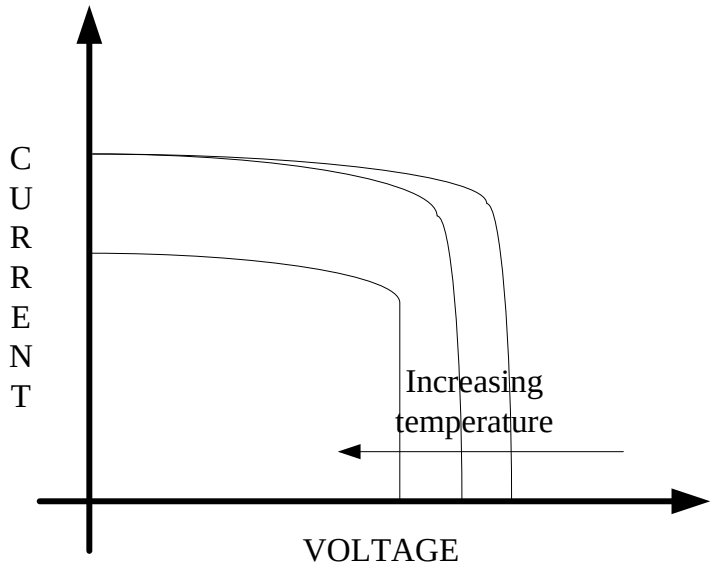

Fig. 4.5: Change in the open circuit voltage with varying temperature.

4.3. PV SIMULATION AT DIFFERENT TEMPERATURES AND INSOLATION

4.3.1 Characteristics at a Temperature of 25^{o}C and 500 W/m^{2}. Figure 4.6 shows the I-V and Fig. 4.7 shows the P-V curves of each solar panel.

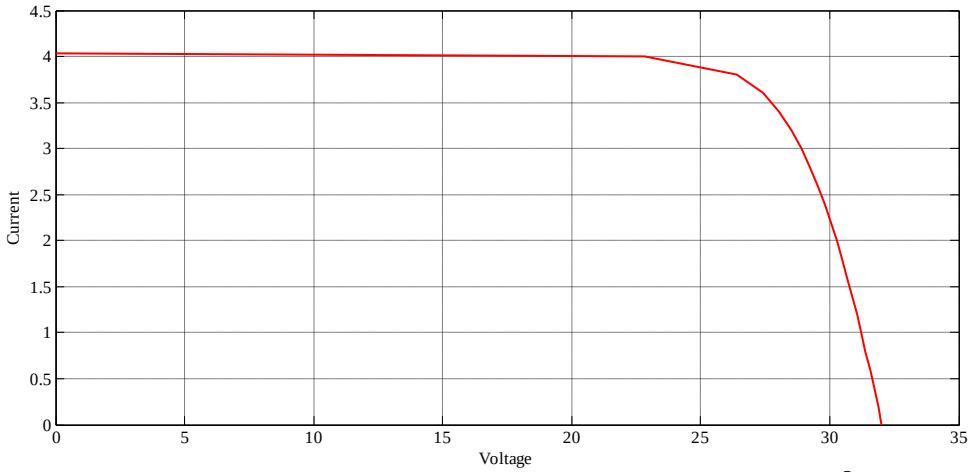

Fig. 4.6: Panel I-V characteristics at 25^{o}C and 500 W/m^{2}.

The short circuit current under these conditions is 4A.with the open circuit voltage at 32.5V.

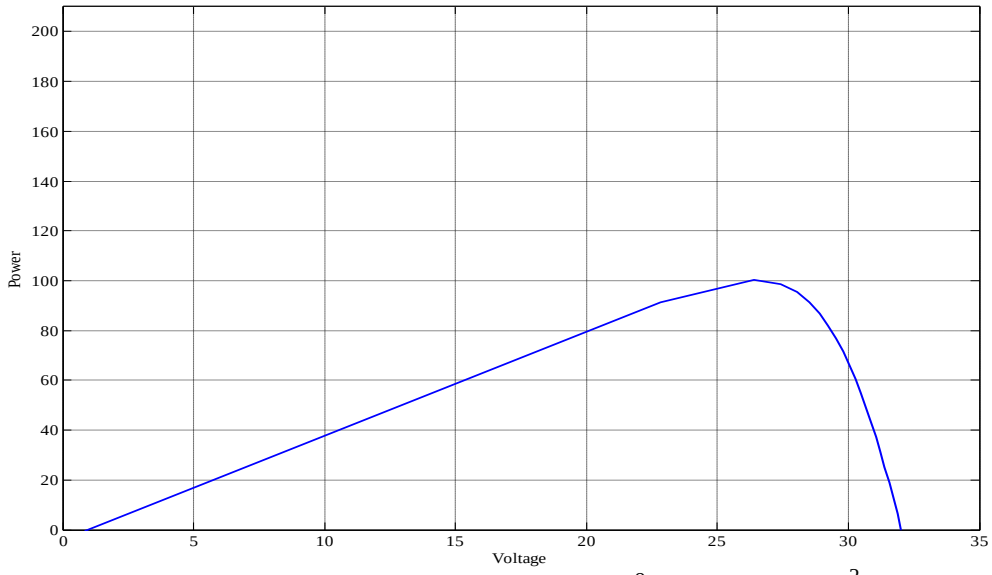

Fig. 4.7: Panel P-V characteristics at 25^{o}C and 500 W/m^{2}.

The maximum power from the panel is 100W.

4.3.2 Characteristics at a Temperature of 35^{o}C and 800 W/m^{2}. Figure 4.8 shows the I-V curve and Fig. 4.9 shows the P-V curve

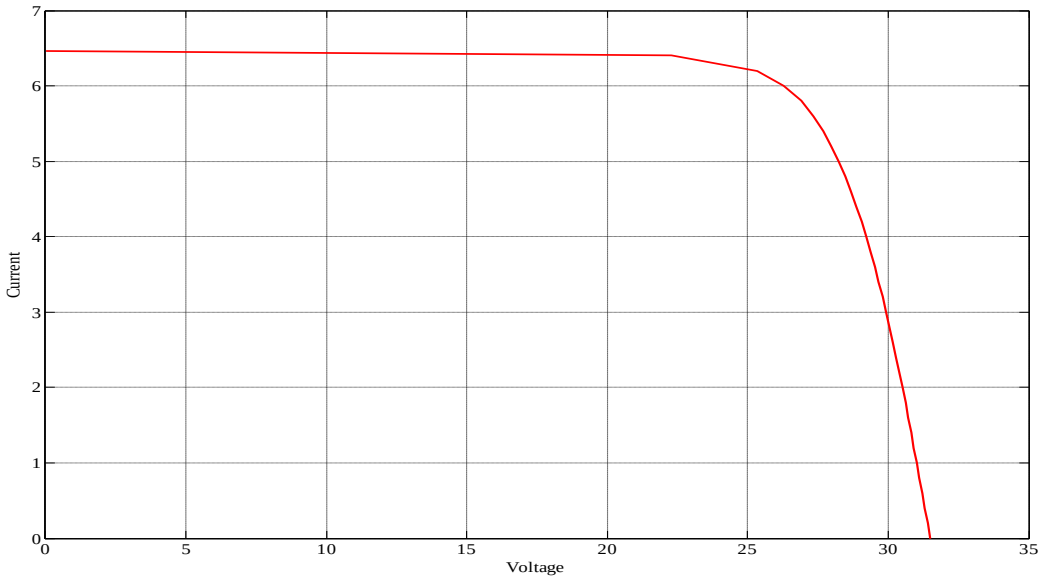

Fig. 4.8: Panel I-V characteristics at 35^{o}C and 800 W/m^{2}.

The short circuit current from the array is 6.5A under these conditions and the voltage is reduced to 32V.

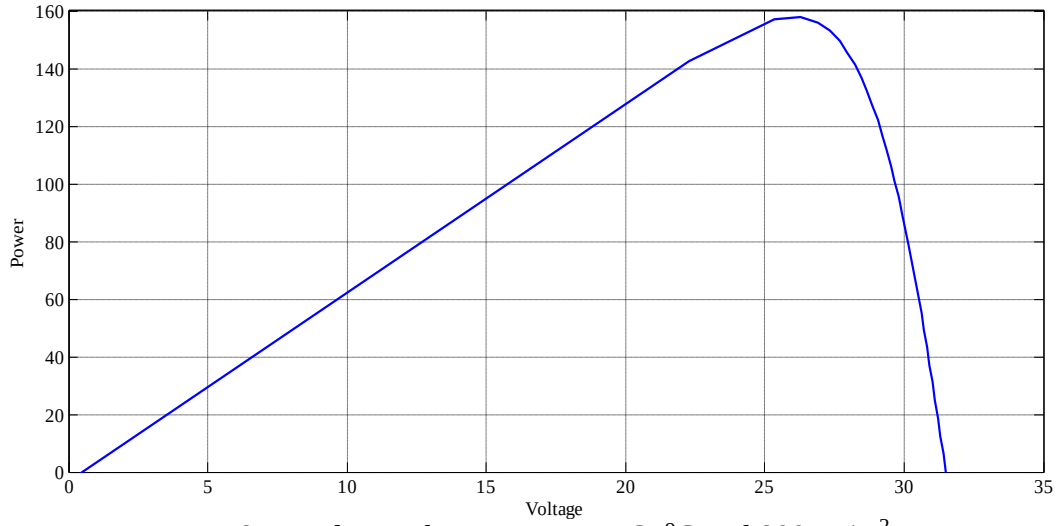

Fig. 4.9: Panel P-V characteristics at 35^{o}C and 800 W/m^{2}.

The maximum power possible from the panel is 160W.

4.3.3 Characteristics at a Temperature of 45^{o}C and 1000 W/m^{2}. Figure 4.10 shows the I-V curve and Fig. 4.11 shows the P-V curve.

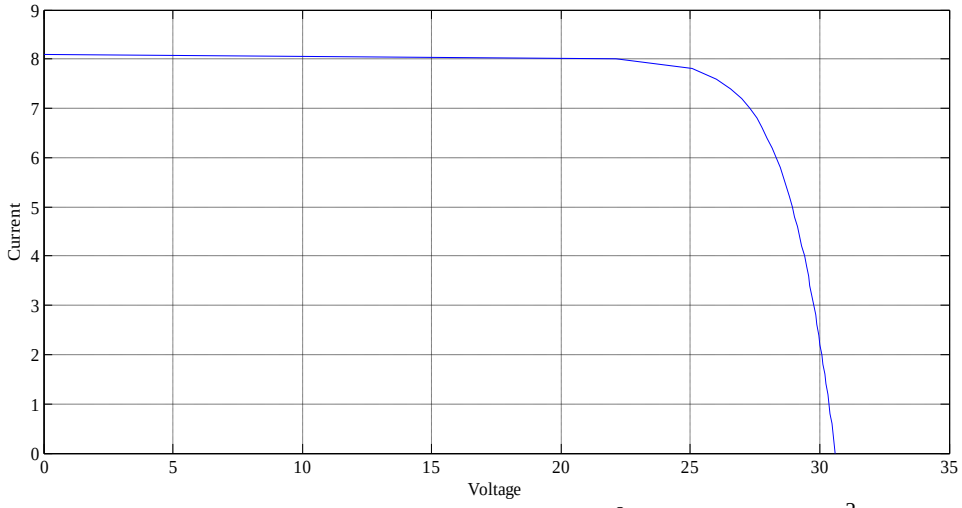

Fig. 4.10: Panel I-V characteristics at 45^{o}C and 1000 W/m^{2}.

As can be observed from the figure above, the short circuit current is 8.1A and open circuit voltage is 31V.

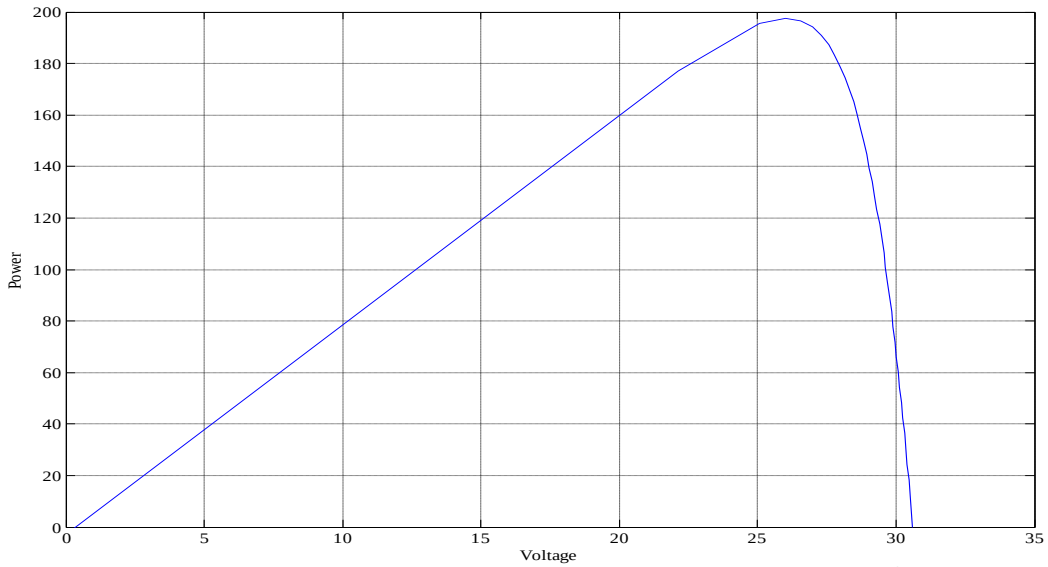

Fig. 4.11: Panel P-V characteristics at 45^{o}C and 1000 W/m^{2}.

The maximum power point is at 200W for the panel under highest insolation which agrees with that specified by the manufacturer.

5. MAXIMUM POWER POINT TRACKER

5.1. NEED FOR MAXIMUM POWER POINT TRACKER

Section 4 had a brief introduction about the need for maximum power point tracker. The I-V characteristics of the solar panel are non linear and vary constantly with temperature and insolation. When the sun's insolation is incident on the panel it may not give its maximum power for that condition without control of the voltage and current. This is achieved using a MPPT control block.

This MPPT control block is integrated with a dc-dc boost converter that is connected to another converter or a load. Studies on the performance of the PV system with MPPT suggest that the losses in the full system are low when compared to one without it [23].

5.2. COMBINATION OF MPPT ALGORITHMS

Various MPPT techniques have been used in the past and each technique works by using separate control variables which usually is the voltage , current of the array and or the duty ratio of the converter. Some techniques are explained by Esram [24]. The most common widely used techniques are the perturb and observe, incremental conductance and the fractional V_{oc} algorithms

Two algorithms have been implemented together in this thesis to achieve the objective of reserve power as mentioned in Section 2. The first being the on-line search algorithm [25] and the second being the modified fractional open circuit voltage method. Both algorithms are discussed in detail in Sections 5.2.1 and 5.2.2, respectively. The on-

line search algorithm is used to track the true maximum power point whereas the modified fractional open circuit voltage method is used to track the pseudo maximum power point on the P-V curve of the array as shown in Fig. 5.1.

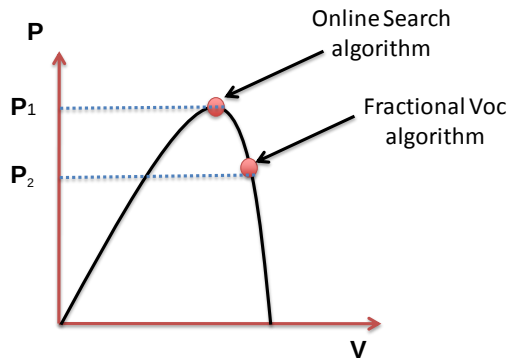

Fig. 5.1: Difference in power P_1-P_2 represents reserve power.

5.2.1 Reserve Power. Point P_1 represents the true maximum power point or the maximum possible power that can be generated for a given insolation whereas point P_2 represents the pseudo maximum power point that has to be tracked by the system. The difference in both the powers that are being generated by the solar array will give the reserve power P_1-P_2 for the array. This reserve power will be used by the solar PV plant in frequency regulation.

5.2.2. On-Line Search Algorithm. The flow chart describing the on-line search algorithm has been shown in Fig. 5.3. The operating current and voltage of the array are constantly monitored and the difference in these variables is checked at every instant of

time. The difference in the value of power is checked between the present and the previous values to determine the sign of the slope on the power characteristic curve. Figure 5.2 shows that the point P_1 is tracked until the slope at the maximum power point is zero. The slope calculated is fed as an error for the reference voltage used for tracking by the algorithm. This process is repeated until the slope is zero.

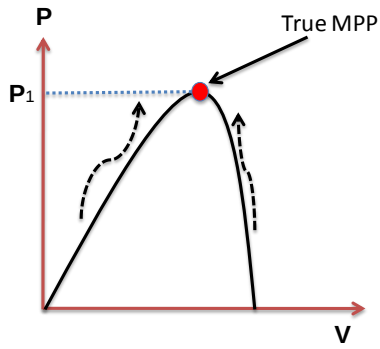

Fig. 5.2: True MPP tracking using on-line search algorithm.

One drawback with the on-line algorithm is that there are oscillations around the MPP. The magnitude of the oscillations is dependent on the step size of the change in the reference voltage. A code has been written in Matlab and is included in Appendix A. In Figs. 5.3 and 5.5, V_{op} and I_{op} represent the instantaneous voltage and current of the array that are monitored by the MPPT block. V_{pv} and I_{pv} used in this thesis refer to the operating values of the voltage and current, respectively, for the PV array at the desired power point.

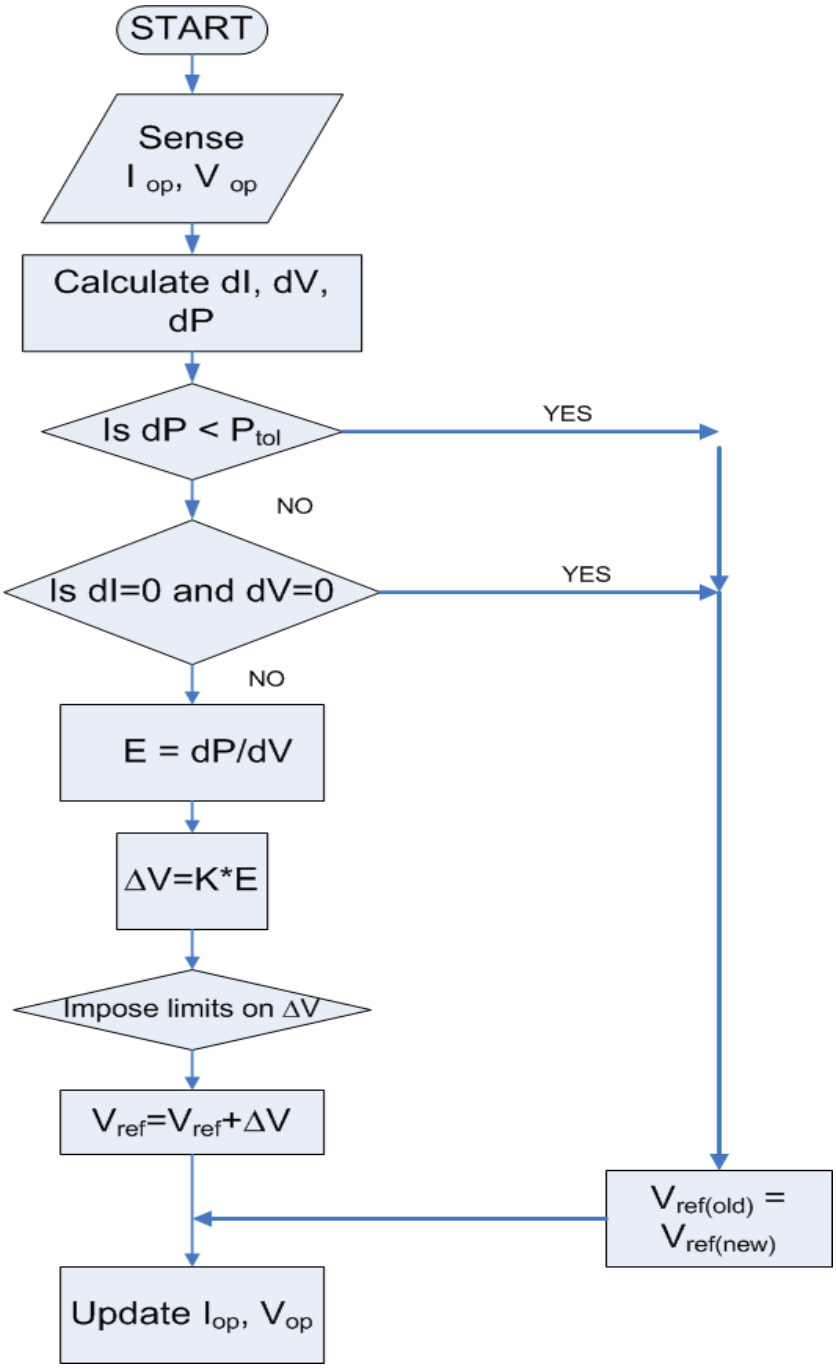

Fig. 5.3: On-line search algorithm.

The error between the operating PV voltage and the reference voltage is fed to a PI block which then generates a control signal which is used as a duty ratio for the dc-dc converter. V_{ref} represents the initial value of tracking voltage for the MPPT.

5.2.3 Modified Fractional Open Circuit Voltage Algorithm. To get the reserve power one has to track a power point below the optimal power point for the array. Thus, the modified fractional V_{oc} method has been adopted. In the conventional fractional open circuit method the maximum power point voltage is represented as a fraction of the open circuit voltage of the array as given by (5.1):

$$V_{mpp} = k \times V_{oc} \tag{5.1}$$

where k is the fraction that varies between 0.71 to 0.78 [25], V_{mpp} and V_{oc} represent the maximum power point and the open circuit voltage, respectively. At every instant the open circuit voltage has to be calculated and then the maximum power point is tracked with the most current value of V_{oc}.

This methodology has been modified in this application such that the fraction is now between 0.2 to 0.7 or 0.8 to 0.95 for which an iterative algorithm is implemented to track this value of open circuit voltage and a lower value of power point. Figure 5.4 depicts the logic for the tracking of a pseudo power point.

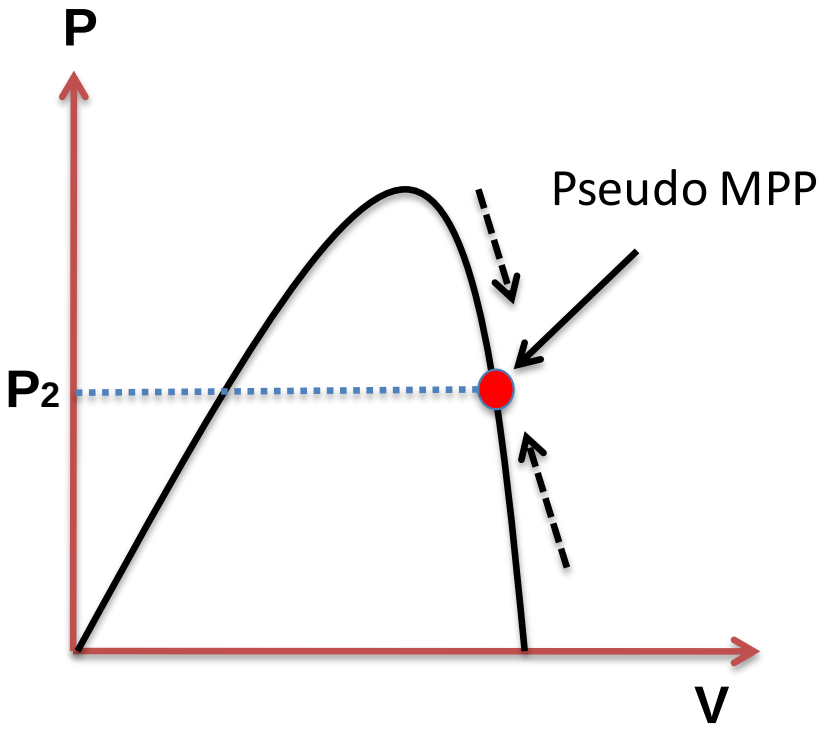

Fig. 5.4: Pseudo power point tracking.

The flow chart that depicts the algorithm is shown in Fig. 5.5. The value k in the decision step of the algorithm is the controlling variable for the amount of reserve power from the PV plant.

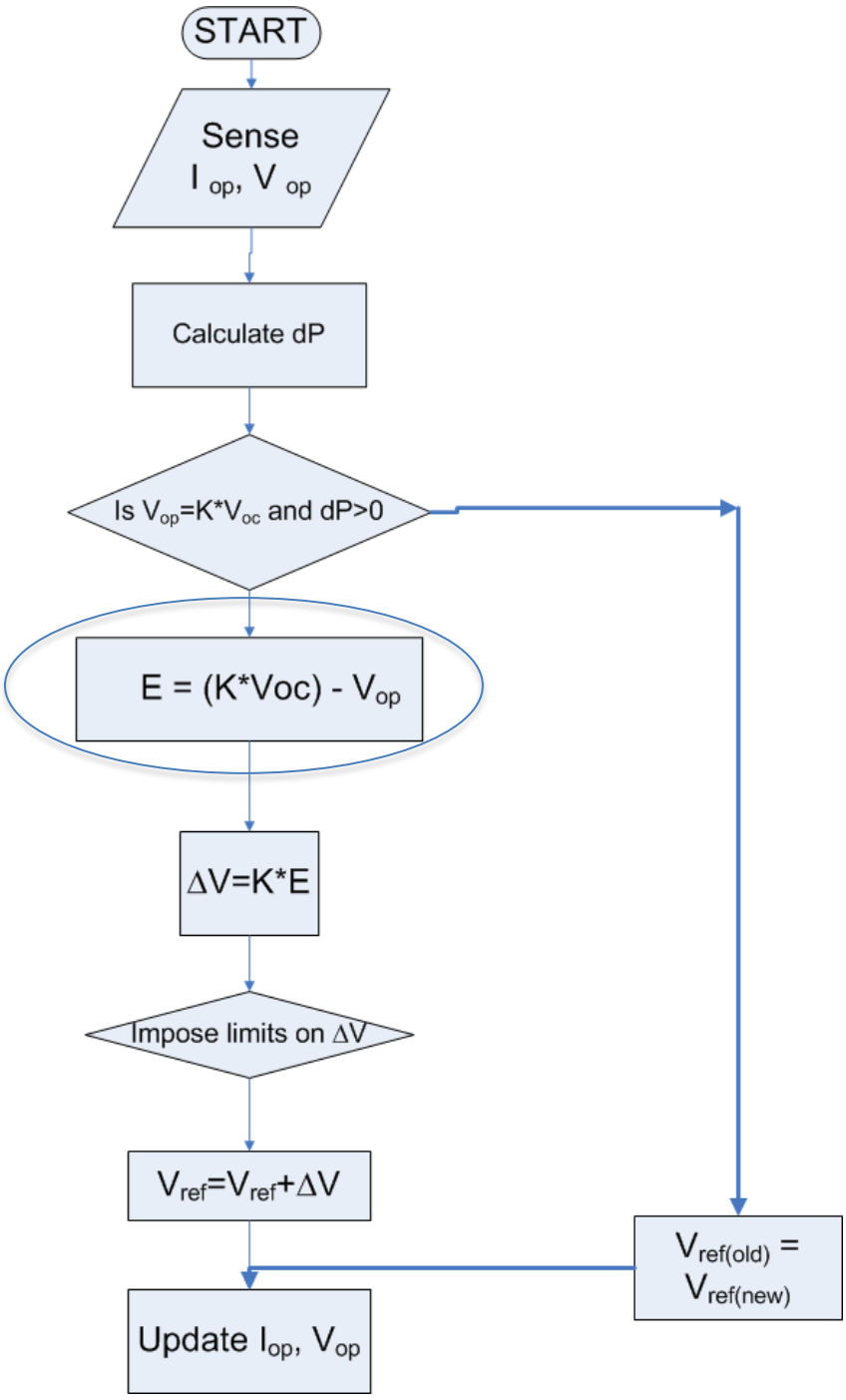

Fig. 5.5: Modified fractional open circuit voltage algorithm.

As shown in Fig. 5.5, the voltage and current of the PV array are constantly monitored and the difference in power between the value at instant (t-1) and (t) is checked if it is greater than zero while the operating point is moved from P_1 to P_2 and the error is the difference between the target voltage value and the operating point voltage. The value of reference voltage is updated with the error value E as marked in Fig. 5.5, which is multiplied by a factor. The Matlab code for the algorithm is included in Appendix B.

Both algorithms are implemented as program modules in the Simulink block for the MPPT. An external signal triggers the change in the algorithm from the true MPP to the pseudo MPP. The sampling time for the current and voltage of the PV system is equal to the time step of simulation of the system. This is to enable the MPPT block to perform the calculation in that time before it receives the next set of voltage and current values. A reference voltage of 125V has been used for this block. Although any value can be chosen as the reference voltage, selecting a number within the limits of the PV system will help the MPPT approach the equilibrium point faster. Figure 5.6 shows the Simulink representation of the MPPT block.

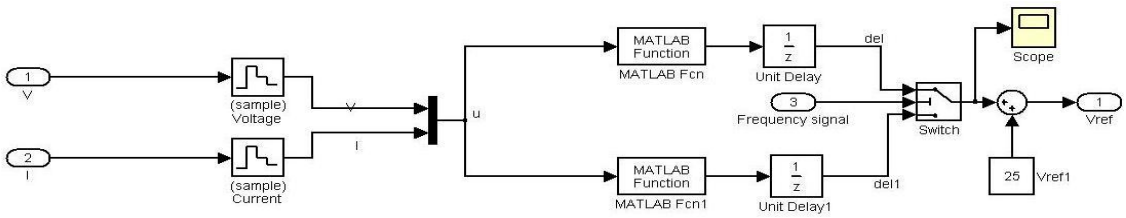

Fig. 5.6: Simulink implementation of the MPPT block.

The effect of change in step values on the convergence of the algorithms and the variation in the duty ratio of the dc-dc converter is discussed in the simulation results section. The outputs of both algorithm control blocks are the change in the reference voltage value. The difference between the V_{ref} and V_{pv} is the error that is fed to the PI block that turns the switch of the converter on and off. The dc-dc converter and the inverter are discussed in detail in Section 6.

6. DC-DC BOOST CONVERTER AND SINGLE PHASE INVERTER

6.1 TOPOLOGY OF THE CONVERTERS

A boost converter has been used to step up the PV voltage and integrate the system to the grid through a single phase inverter. Since the voltage output of the PV system is low, using a boost converter is helpful in stepping up the voltage and using it for different applications like charging a battery. Figure 6.1 shows the topology of the converters used in the thesis, they have been designed using PLECS version 3.0.2.

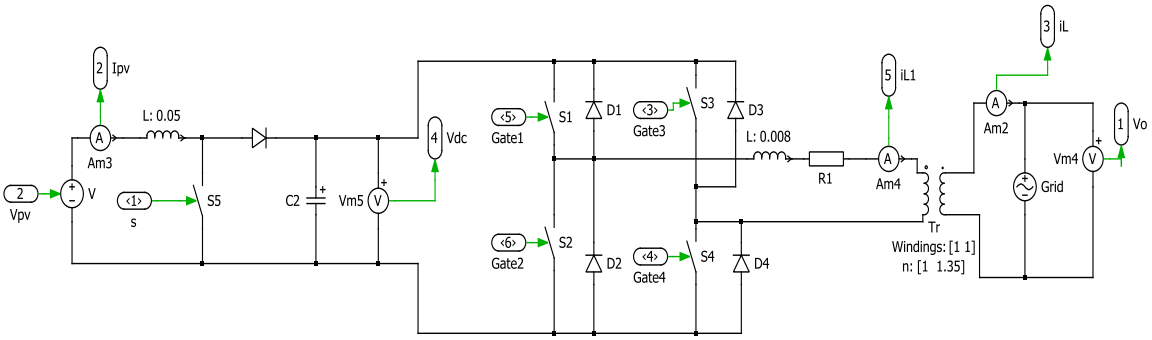

Fig. 6.1: Boost converter and single phase inverter.

The output voltage for the boost converter is 260V dc and this is converted to 260V p-p ac using the single phase inverter. A transformer is used to step up the voltage to that of the grid to 340V peak. A high value of capacitance, equal to 1000μF, has been used at the dc output to maintain a stiff voltage at the terminals. Frequency of switching is 30kHz.

The inductor value for the boost converter is 0.05H. The transformer turns ratio is 1:1.32 to step the voltage from 260V to 340V peak or above to make the system capable of injecting power in the grid. .

6.2 BOOST CONVERTER AND INVERTER

Pulse width modulation (PWM) has been used for the switching of the boost converter. The switching is done with a carrier wave of frequency 30 kHz that takes the voltage error from the PI block as a control voltage input.

6.2.1 Design Considerations. Assuming continuous conduction for the current calculation of inductor and capacitor values is done using the equations as shown

$$\Delta V_c = I_o(V_o - V_s) / (V_o \times f \times C) \tag{6.1}$$

$$\Delta I = (V_o - V_s) \times V_s / (f \times L \times V_o) \tag{6.2}$$

Equation (6.1) is the ripple in the capacitor voltage for the converter, a ripple value of 1% is taken for calculation purposes. In Equation (6.2) ΔI is the ripple in the inductor current, V_o and V_s are the output and input voltages, respectively, f is the frequency of switching, L is the inductance value. A ripple of 10% is considered for the current to calculate the element values [26]. Inductor and capacitor values calculated are C = 255 μF and L = 0.44 mH. But since the boost converter is integrated with the inverter

a higher value of capacitance was chosen to maintain a stiff dc link voltage and to reduce the ripple to about 1.5% (3 to 4V) at the terminals.

6.2.2 Inverter Control. The Simulink design is as shown in Fig. 6.2 was designed using a delta modulation based current control [27]. The inverter controller is a type of PWM switching for the switches. It takes the grid voltage, grid current and the dc link voltage error as inputs to switch such that the power from the PV system is injected at unity power factor.

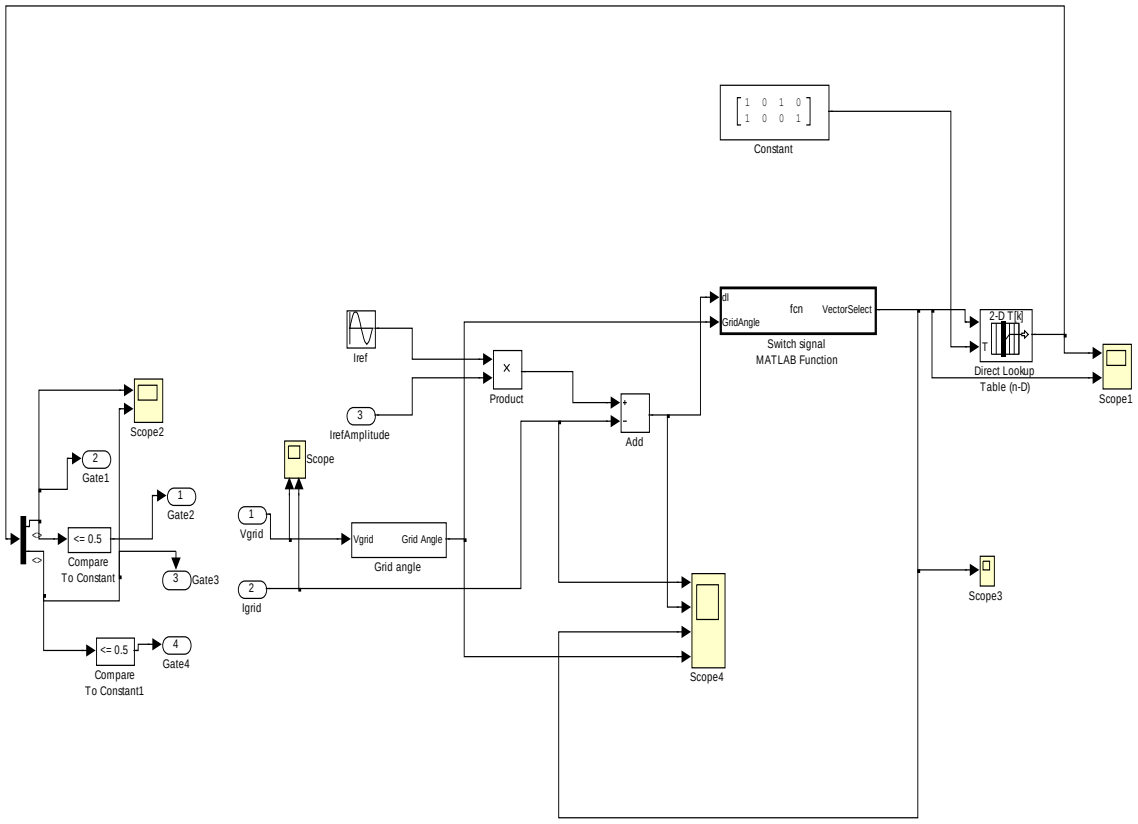

Fig. 6.2: Inverter control block.

For effective control of the inverter switching in a two stage power conversion system it has a closed loop control which takes in the grid voltage, current and the dc bus reference voltage as inputs and controls the gate signals to transfer the power at unity power factor [28]. I_{ref} which is the error of the dc link voltage is multiplied with a sine wave for using it as a reference to check if the current in the grid is increasing or decreasing. Based on the sign of the difference dI and the sign of the grid voltage angle the power injected into the grid is varied.

For same sign of the grid voltage angle and dI, the inverter switches inject power else they bypass the input source. The Matlab code for the control logic of the switches is given in Appendix C. Implementation of a closed loop control for the inverter is essential to have an effective control over the amount of power being given by the inverter to the grid [29-31]. Injected power and the variation under different power generation from the PV system are discussed in Section 7.

7. SYSTEM AND SIMULATION RESULTS

7.1. TEST SYSTEM

Analysis and study of the complete system is done under various scenarios and has been presented as different cases in this section. Each case simulation has been done in Matlab/Simulink R2008b. Figure 7.1 shows the complete topology of the two stage power conversion with photovoltaic system at the input. Different parameter values for each case have been described in their respective sections. Various conditions such as constant insolation, uniformly varying and non-uniform ly varying insolation have been evaluated.

A GE PV 200W solar panel was used as the building block for the 2kW array. An external signal to simulate the change in frequency was implemented.

While a change in inertia for conventional generators helps in restoring the frequency, solar power plants are shown to respond in a similar fashion by inverter control. The reserve power from the PV plant acts in a manner analogous to the inertia. The PV system is made to operate initially at the true power or pseudo power mode based on the requirements from the generation plant.

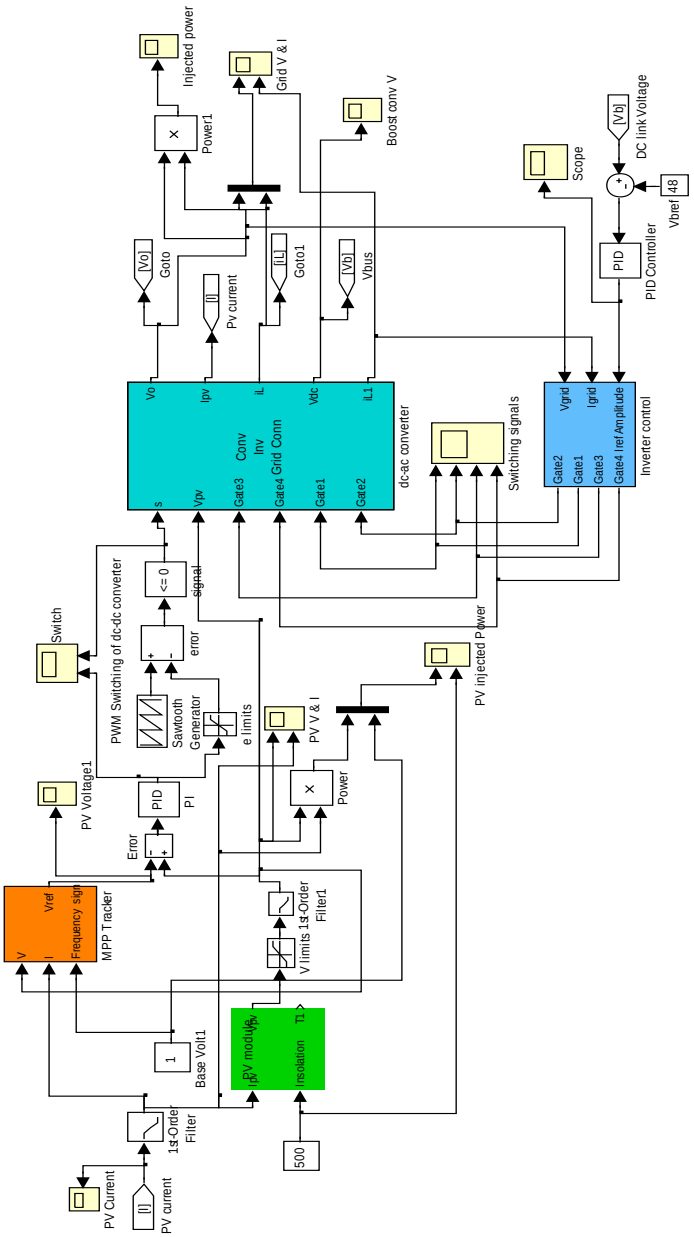

Fig. 7.1: Complete system topology in Simulink.

As shown in Fig. 7.1, two separate control blocks, one for the boost converter and the other for the inverter have been designed. The inverter's control block can be used to

inject the reactive power into the grid side by implementing a phase difference in the reference current input.

The variation of power level at the PV plant is very useful in following the load demand. This, variation in power levels is shown in several cases with respect to a true maximum power point and a pseudo maximum power point. Discussions of the results obtained and some important observations for each case provided in the next section.

7.2 SIMULATION RESULTS

For the pseudo maximum power mode the k value in the modified fractional open circuit voltage algorithm is 0.95. Any value below 0.7 (left side of P-V curve) or above 0.8 (right side of P-V curve) would help in getting a reserve power margin in the system. A value of 0.95 is chosen to show a significant margin of reserve power for the given insolation.

7.2.1 Case A. Simulation is done at an insolation level of 800W/m^2 and a temperature of 25^{o}C. The power in this case is injected at unity power factor into the grid. Figure 7.2 shows the voltage and current from the PV under two different modes of operation i.e. true maximum power and pseudo maximum power.

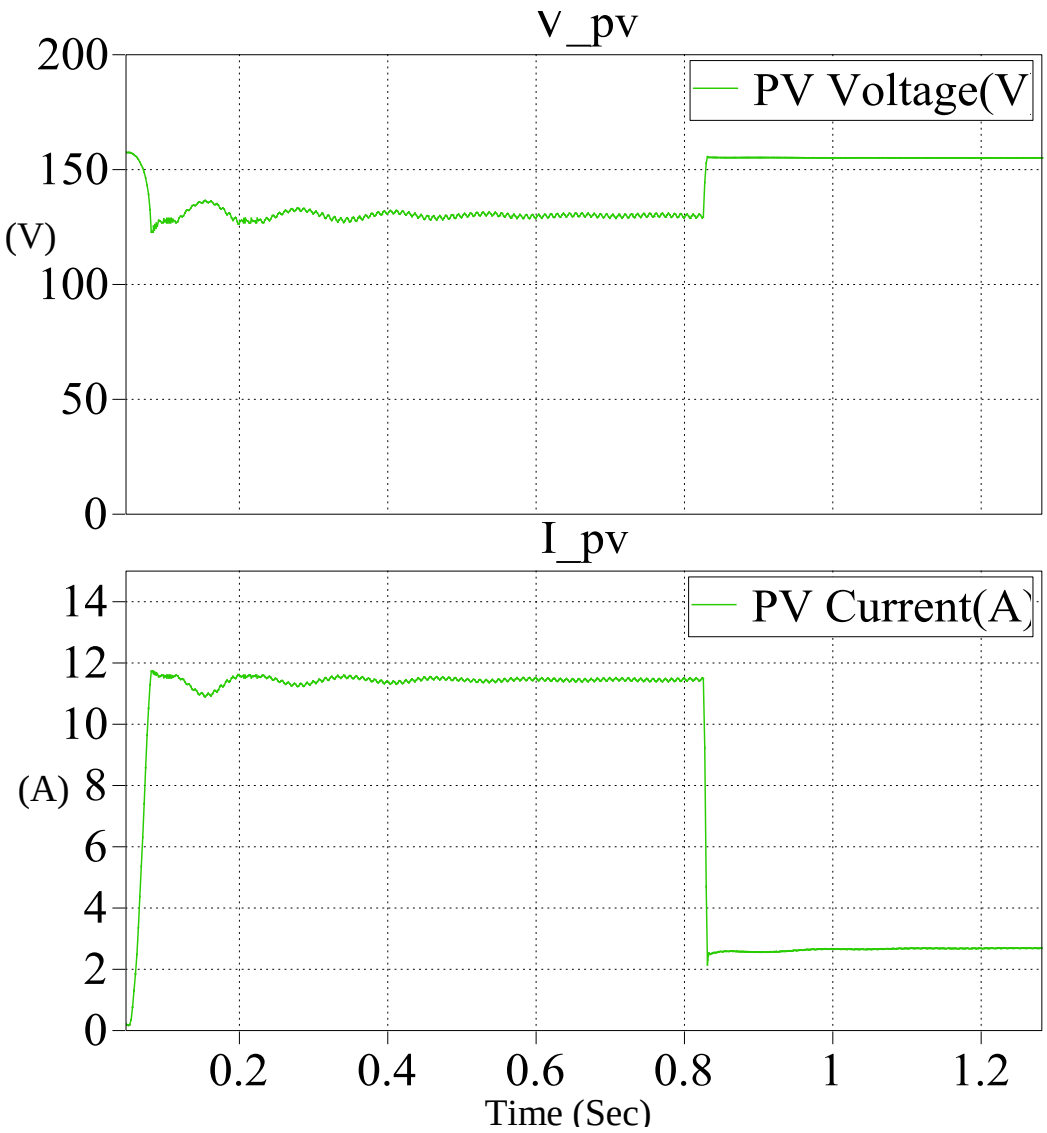

Fig. 7.2: PV voltage and current.

The voltage is at 156V for the pseudo power point and 131V for true maximum power point conditions. Corresponding to the change in voltage, there is a decrease in current from 11.3A to 2.8A.

In Fig. 7.3 for a value of k as 0.95, the average power output is 400W, when the mode of operation is under true power conditions the output is 1490W. The change in

mode is triggered by the external frequency change signal at 0.82 sec. In an actual system, the signal will be derived from an aggregate frequency response characteristic of the system load demand.

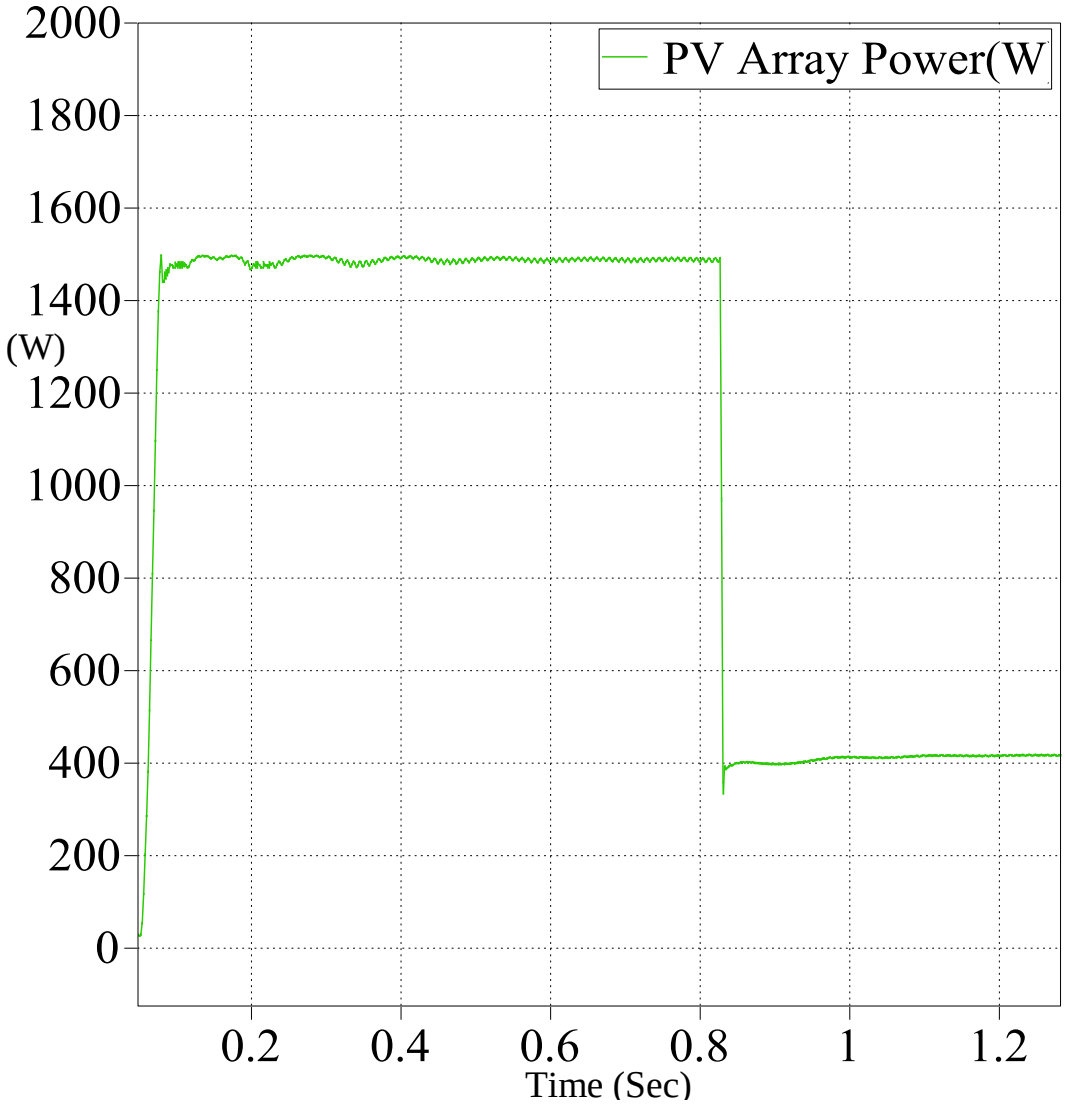

Fig. 7.3: Change in PV output power for 800 W/m^2.

Figure 7.4 shows the boost converter's output voltage for the entire operating time of the system. Although there is a ripple of 4V, the average value of the output is 260V. One should have such a constant dc bus voltage to have control over the power transferred from source to the grid. There is a spike in the voltage waveform at t = 0.85 sec due to the change in the operation mode of the system, however it settles down to the average value of 260V after 0.2 sec.

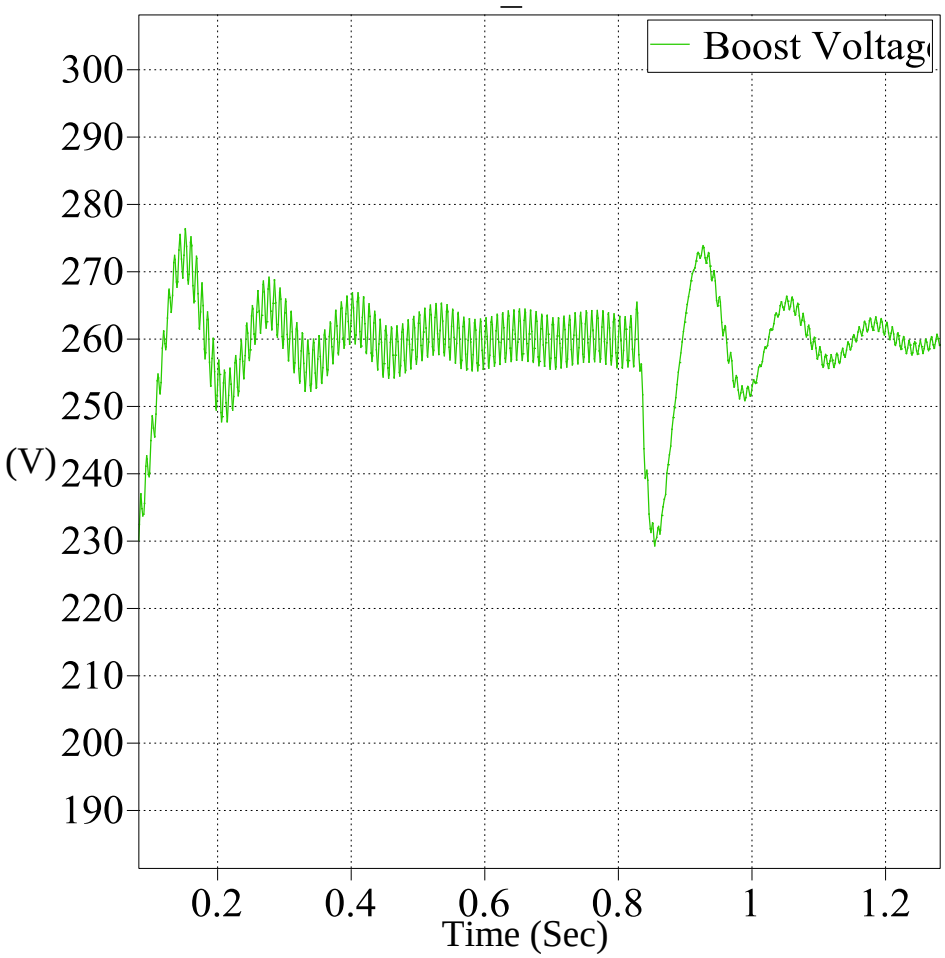

Fig. 7.4: Boost converter output voltage.

Figures 7.5 and 7.6 are the zoomed sinusoidal waveforms of the injected current at the grid side for the two power modes. 8.75A and 2.35A of current is being injected at a grid voltage of 340V peak to peak for a power of 1490W.

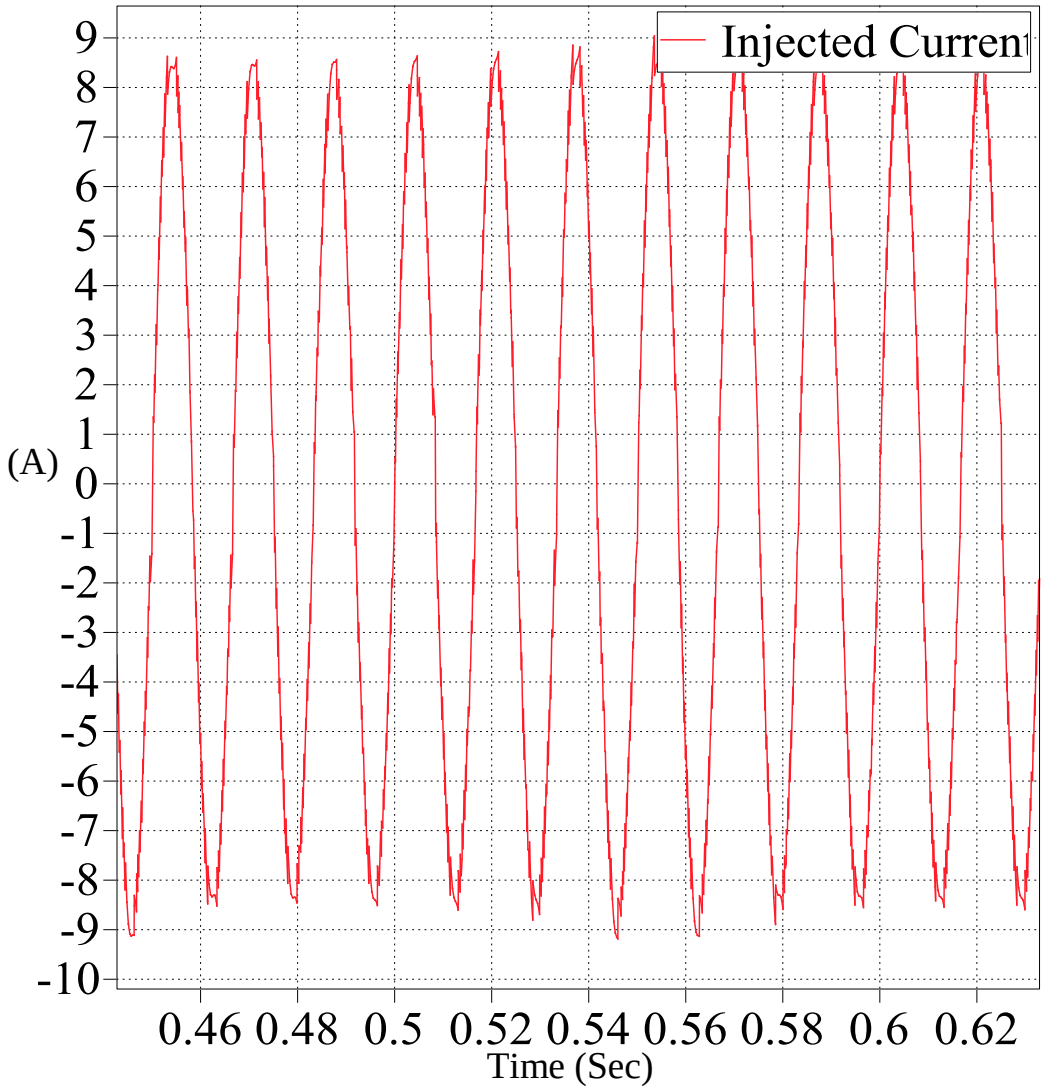

Fig. 7.5: Current injected into the grid at 1490 W (True MPP).

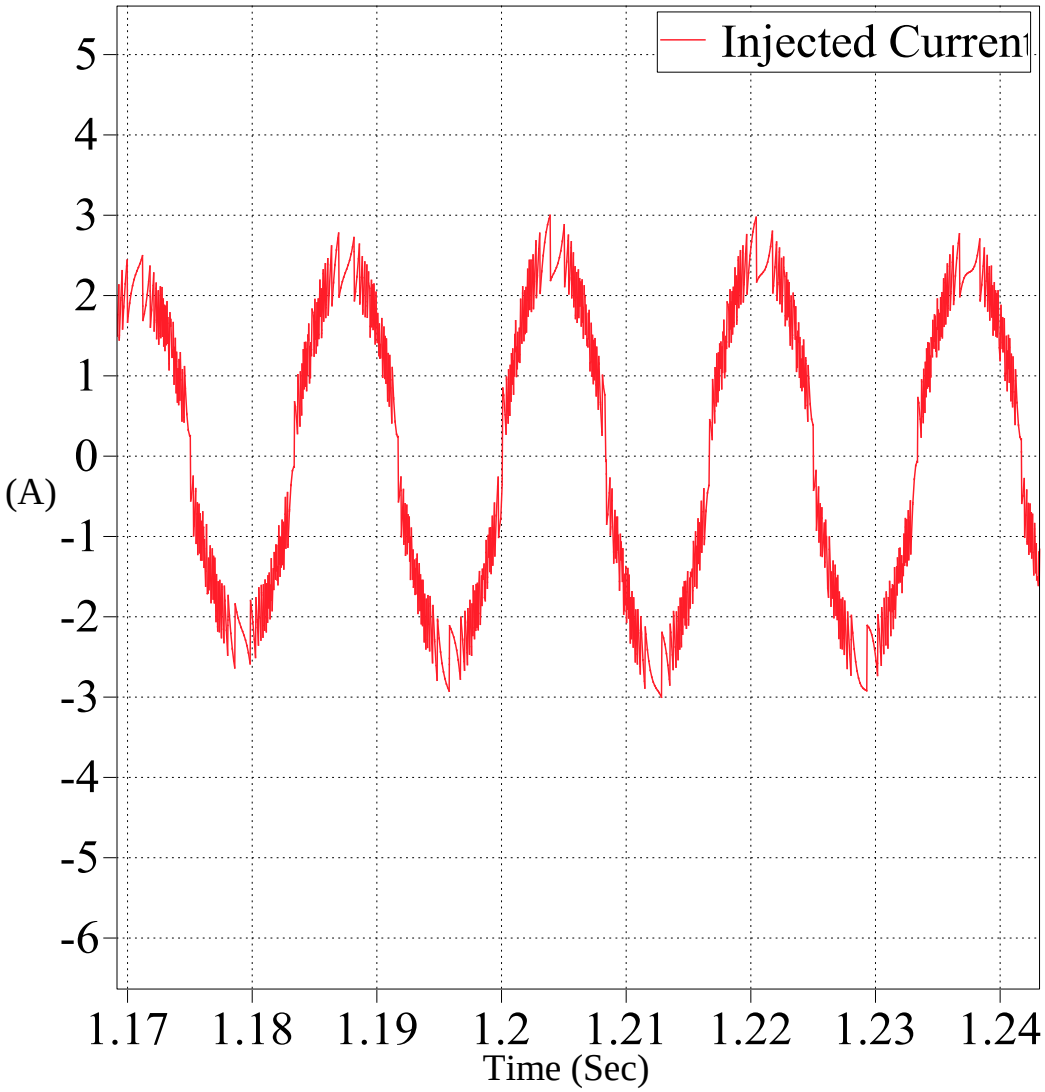

Fig. 7.6: Current injected into the grid at 400W (Pseudo MPP).

Figure 7.7 shows the stiff voltage at the grid side at which the PV system is supplying the power generated at unity power factor. This is the value of the voltage at which the power is being delivered on the grid side for all the cases discussed.

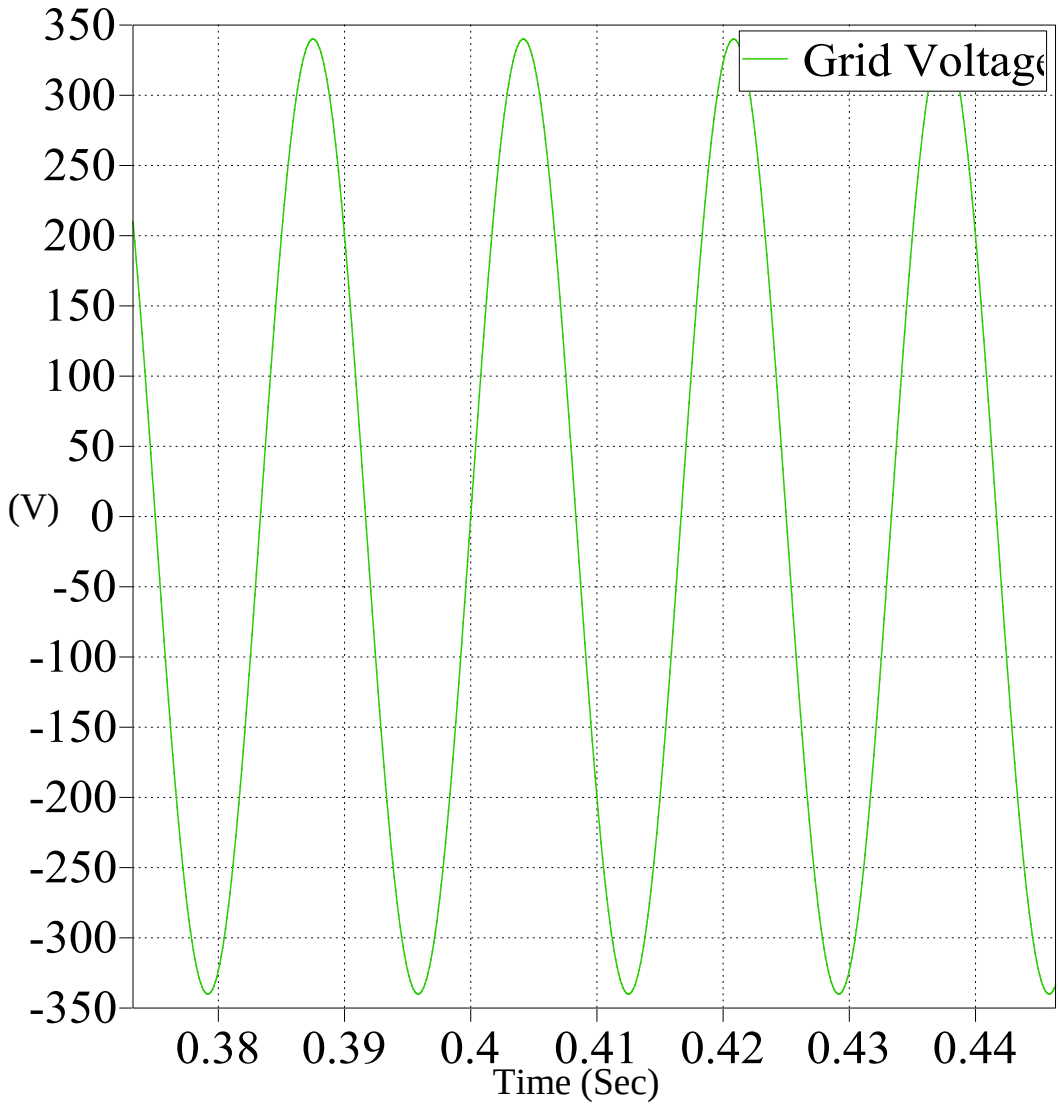

Fig. 7.7: Voltage of the grid (340V p-p).

Figures 7.8 and 7.9 show the power on the output side of the inverter. As can be observed the power is at unity power factor, since it is completely positive indicating that voltage and current are in phase with each other.

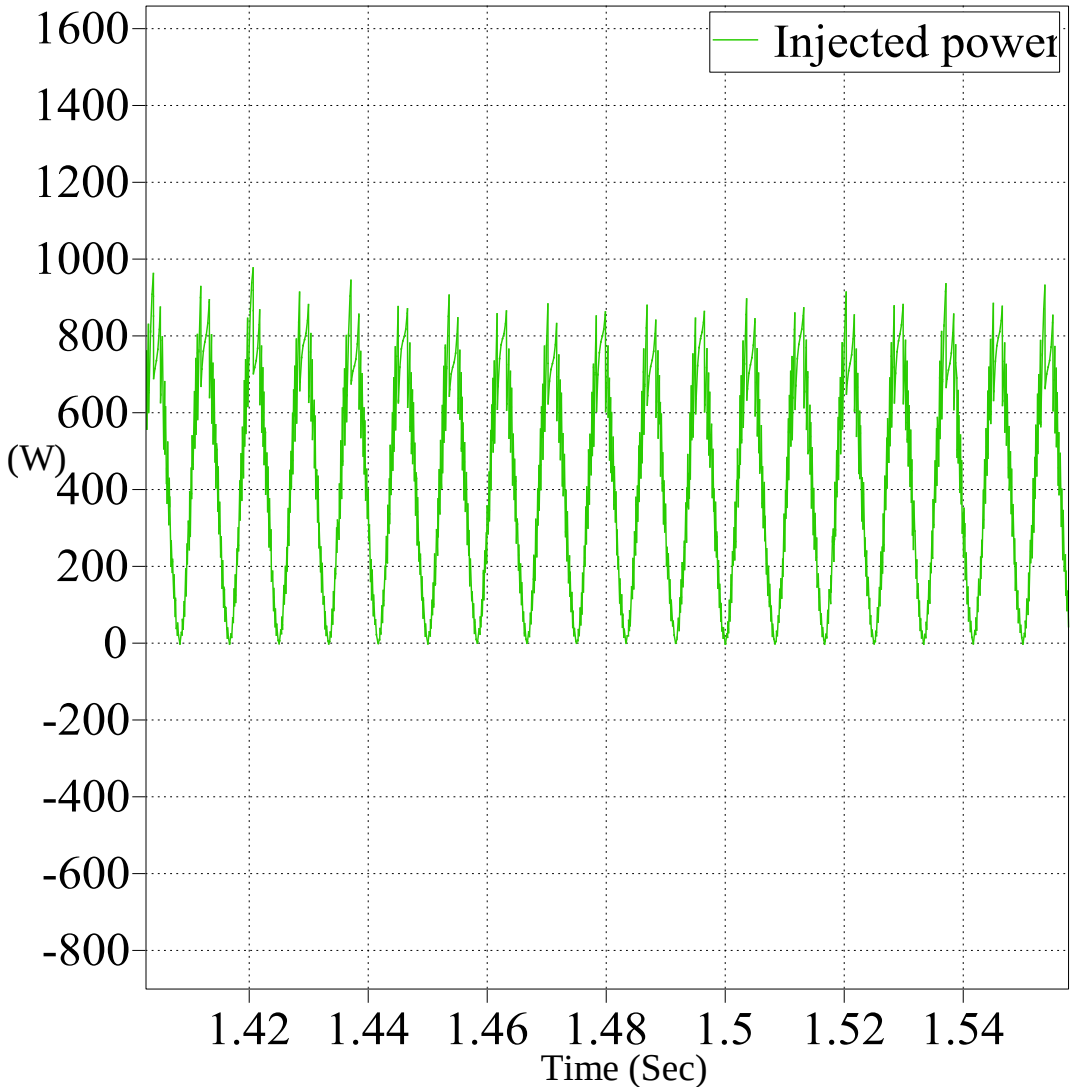

Fig. 7.8: Average power of 400W being injected into the grid for pseudo MPP.

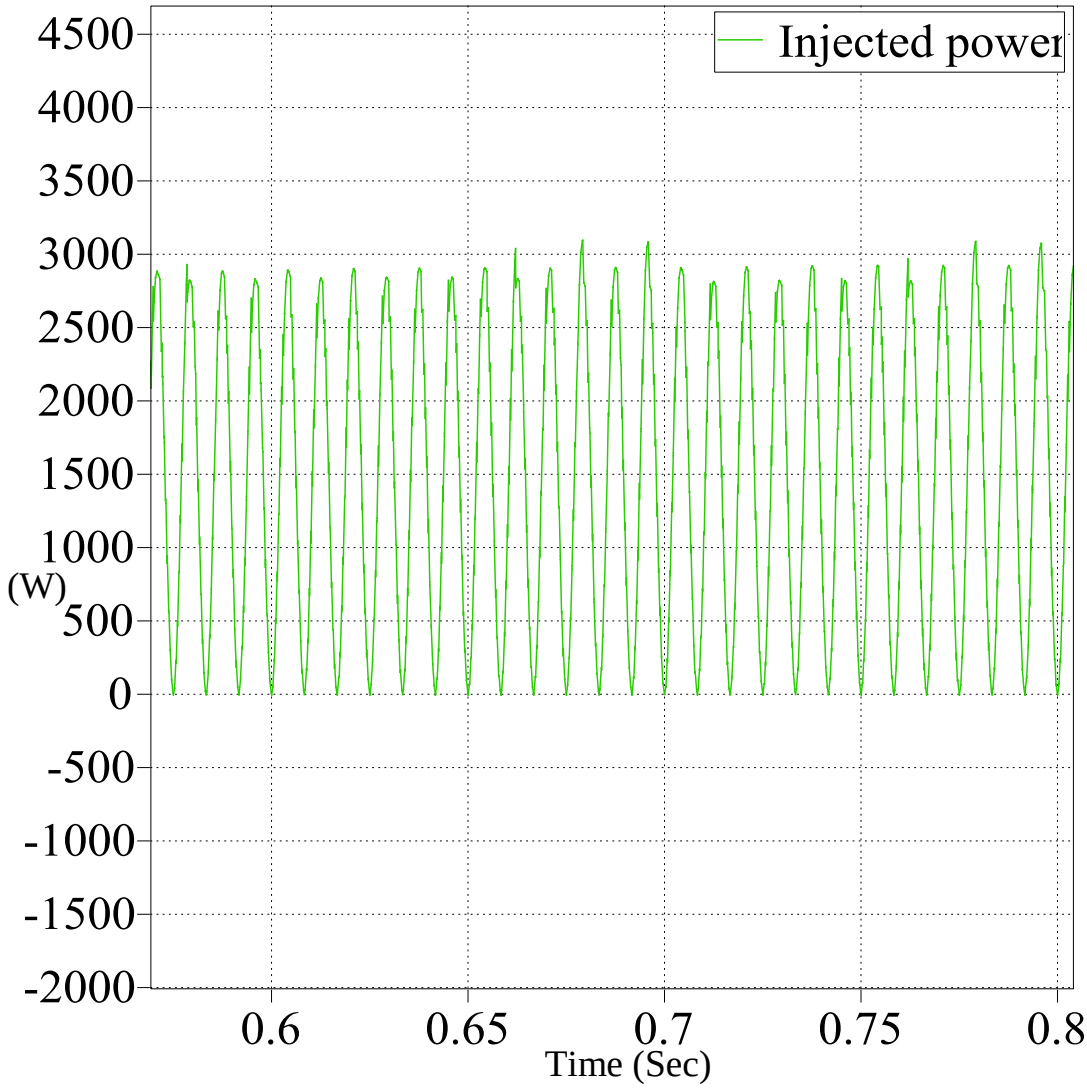

Fig. 7.9: Average power of 1490W being injected into the grid for true MPP.

Figure 7.10 shows the active power on the grid end for true maximum power. It can be observed that initially there are few oscillations which dampen out after about 0.5 sec and give a constant output.

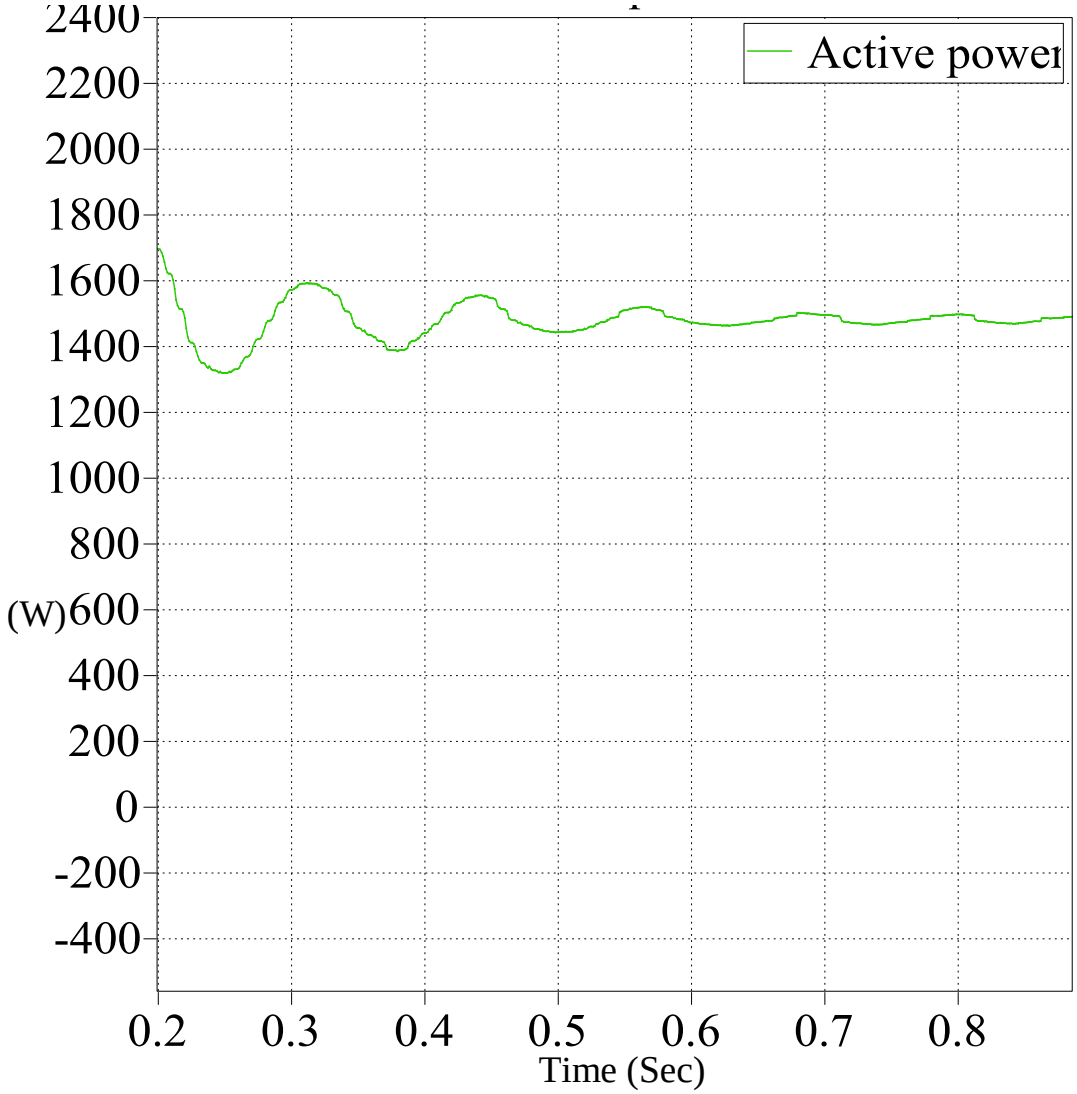

Fig. 7.10: Active power curve for true maximum power at 800 W/m^2.

Figure 7.11 shows zoomed graph of the active power curve for pseudo maximum power. Under this mode also, the system has oscillations initially, but dampens out after 0.25 sec to give a constant output.

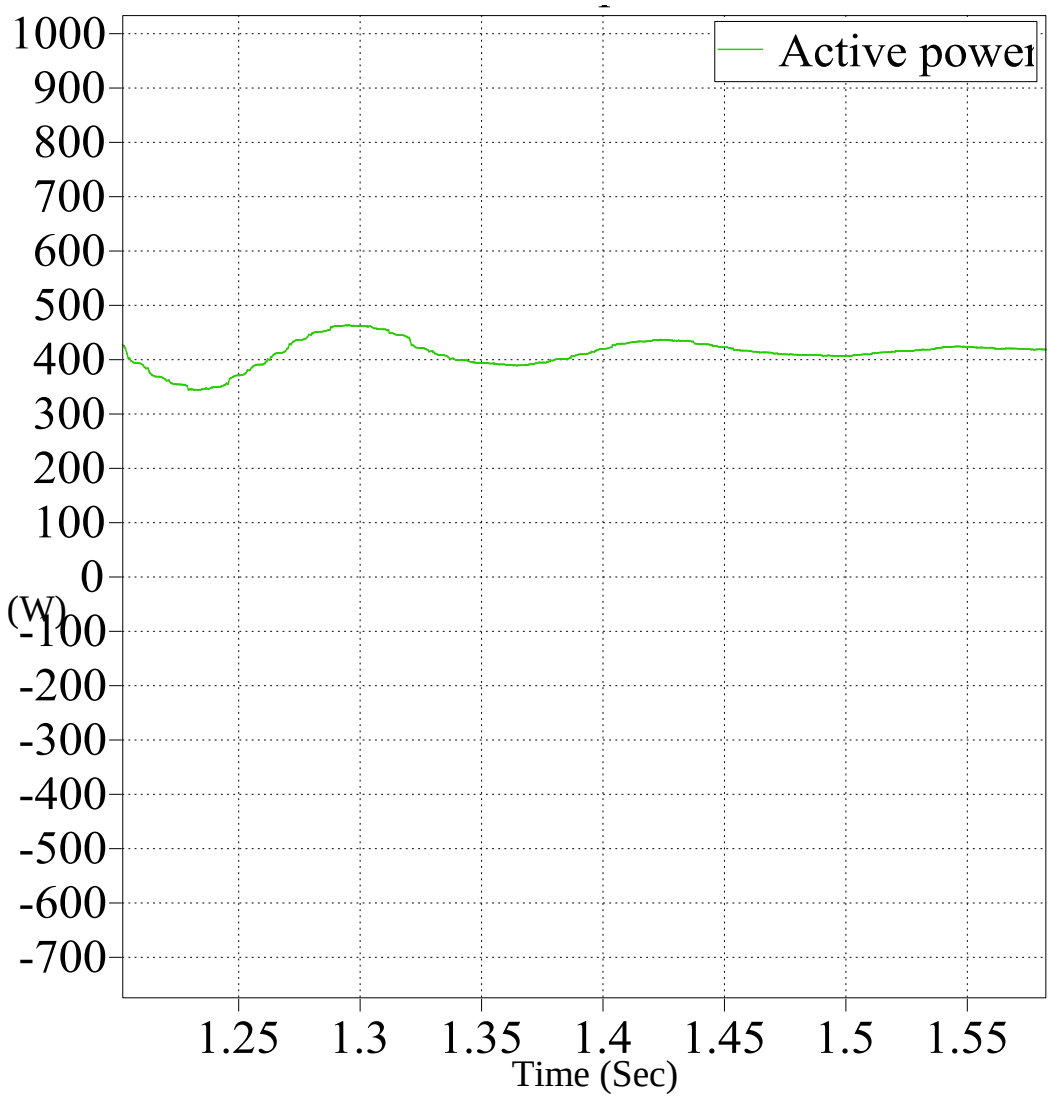

Fig. 7.11: Active power curve for pseudo maximum power at 800 W/m^2.

7.2.2 Case B. Insolation is 1000 W/m^2 and temperature is 35^{o}C. The system is again checked for pseudo and true power mode and the outputs at the grid are analyzed.

At this temperature the effective open circuit voltage for the PV system changes as per Equation (4.3). The new open circuit voltage is now 158.5V since there will be a drop of 6V now for 5 panels connected in one string. So for tracking the pseudo power

point the voltage to be tracked now is 0.95*158.5 = 150.57V. Figure 7.12 shows the variation in the PV voltage and current for two power modes. This case shows the sudden variation in the PV power from high to low and vice versa. It can be observed that the response to a change in power level is fast when changing from one mode to another.

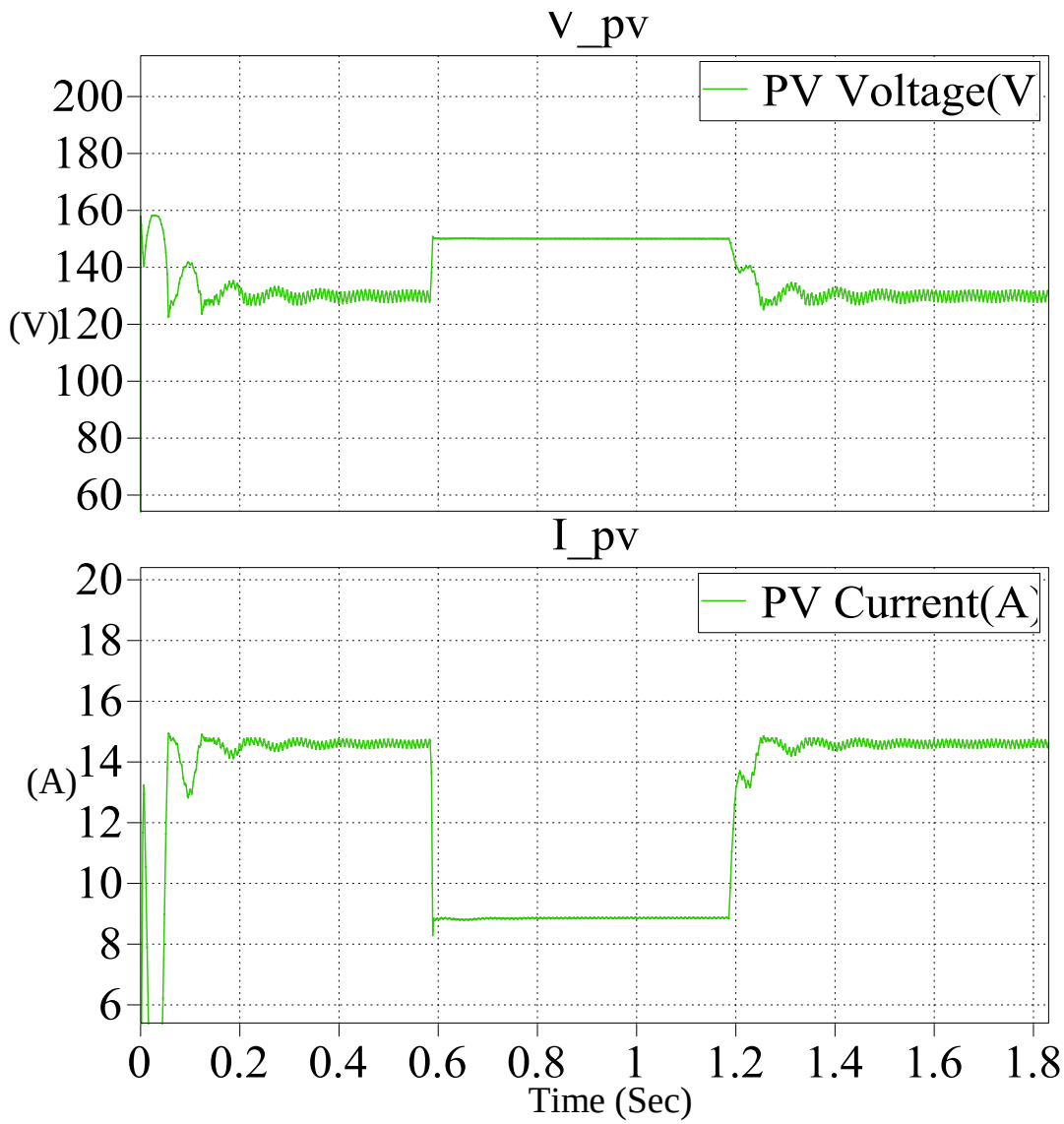

Fig. 7.12: PV voltage and current.

Voltage value changes between 131V and 150V while the current changes from 14.5A to 8.85A for different power levels. This will enable the system to respond fast to sudden variations in load. Figure 7.13 shows the variation in output power of the PV array at 1000W/m^2.

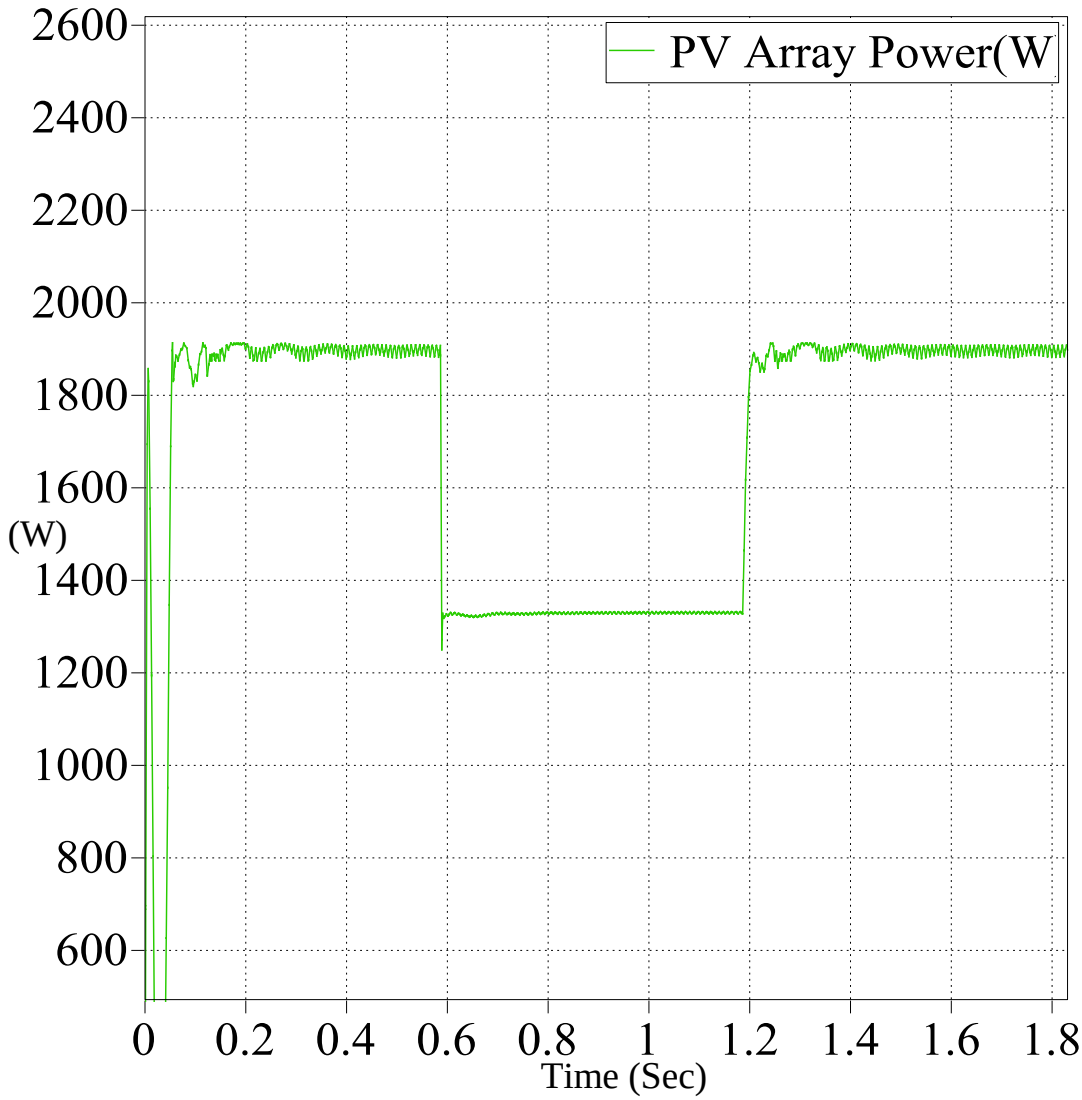

Fig 7.13: Change in PV output power for 1000 W/m^2.

With a change in the grid frequency, the power generation from the solar array is increased or decreased whether the frequency has dropped or risen.

Figures 7.14 and 7.15 show the zoomed graphs of the current injected at the grid end for high power (11.2A) and low power (7.85A) modes. Since the temperature is at a higher value than nominal there is a slight variation in the maximum power that is being generated by the solar array for maximum possible insolation.

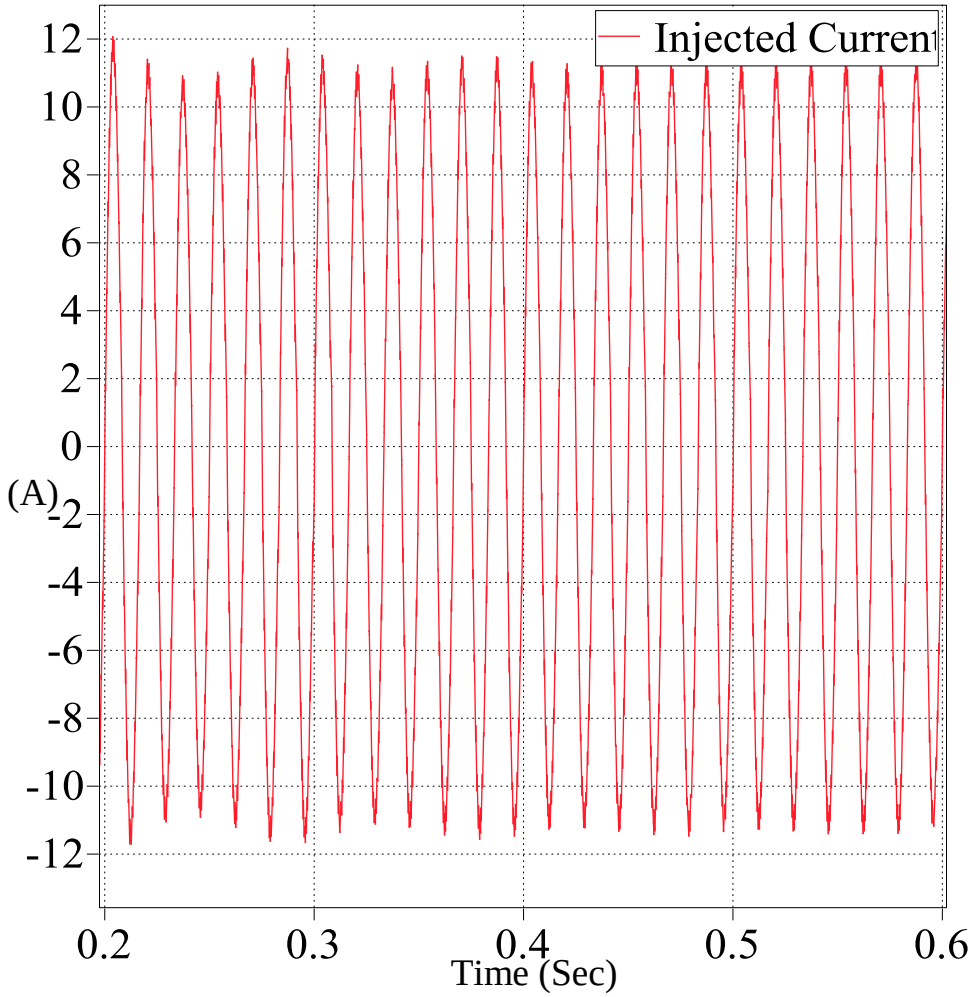

Fig. 7.14: Current injected into the grid side for 1910W (True MPP).

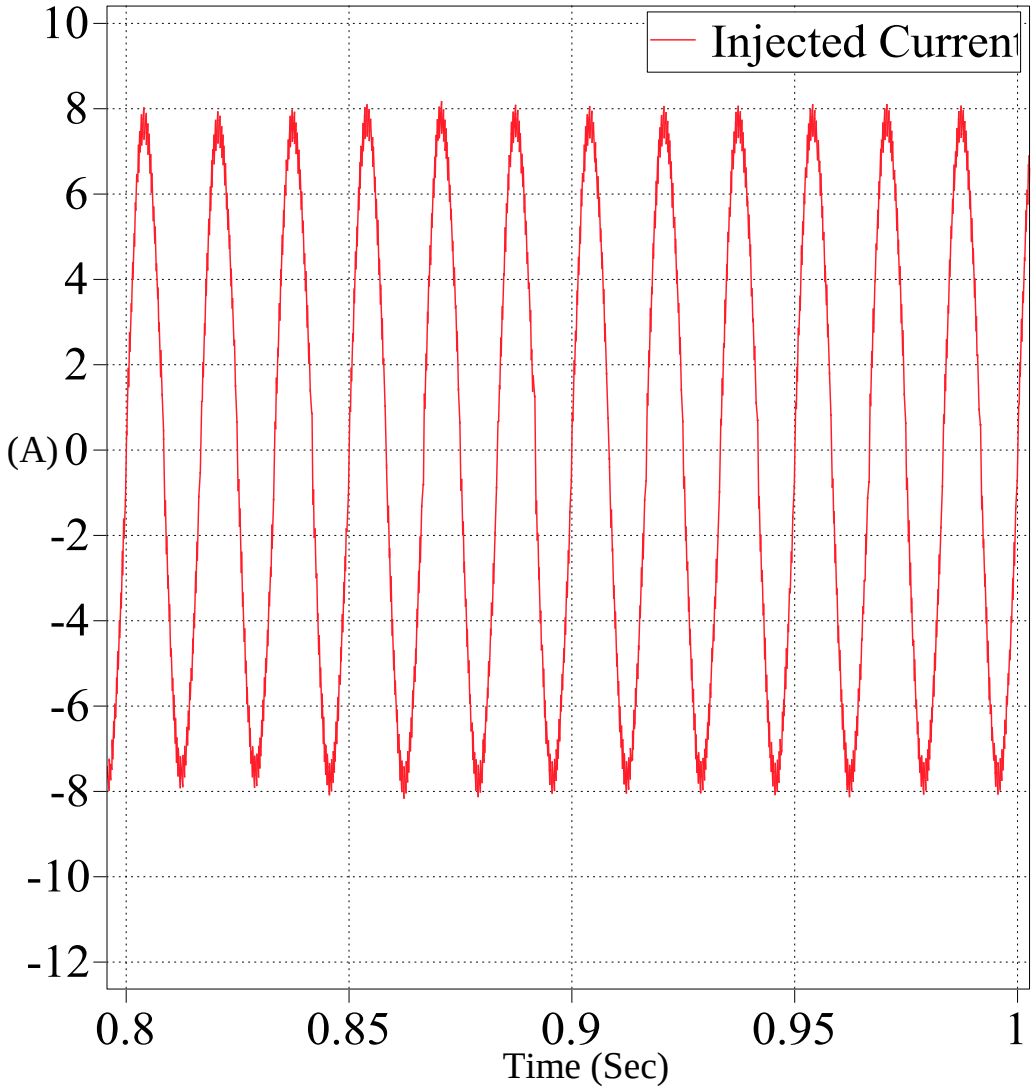

Fig 7.15: Current injected into the grid side for 1330W (Pseudo MPP).

Power is injected into the grid at unity power factor. The net power is positive indicating that the voltage and current are in phase with each other as shown in Figs. 7.16 and 7.17 with average powers at 1910W and 1330W.

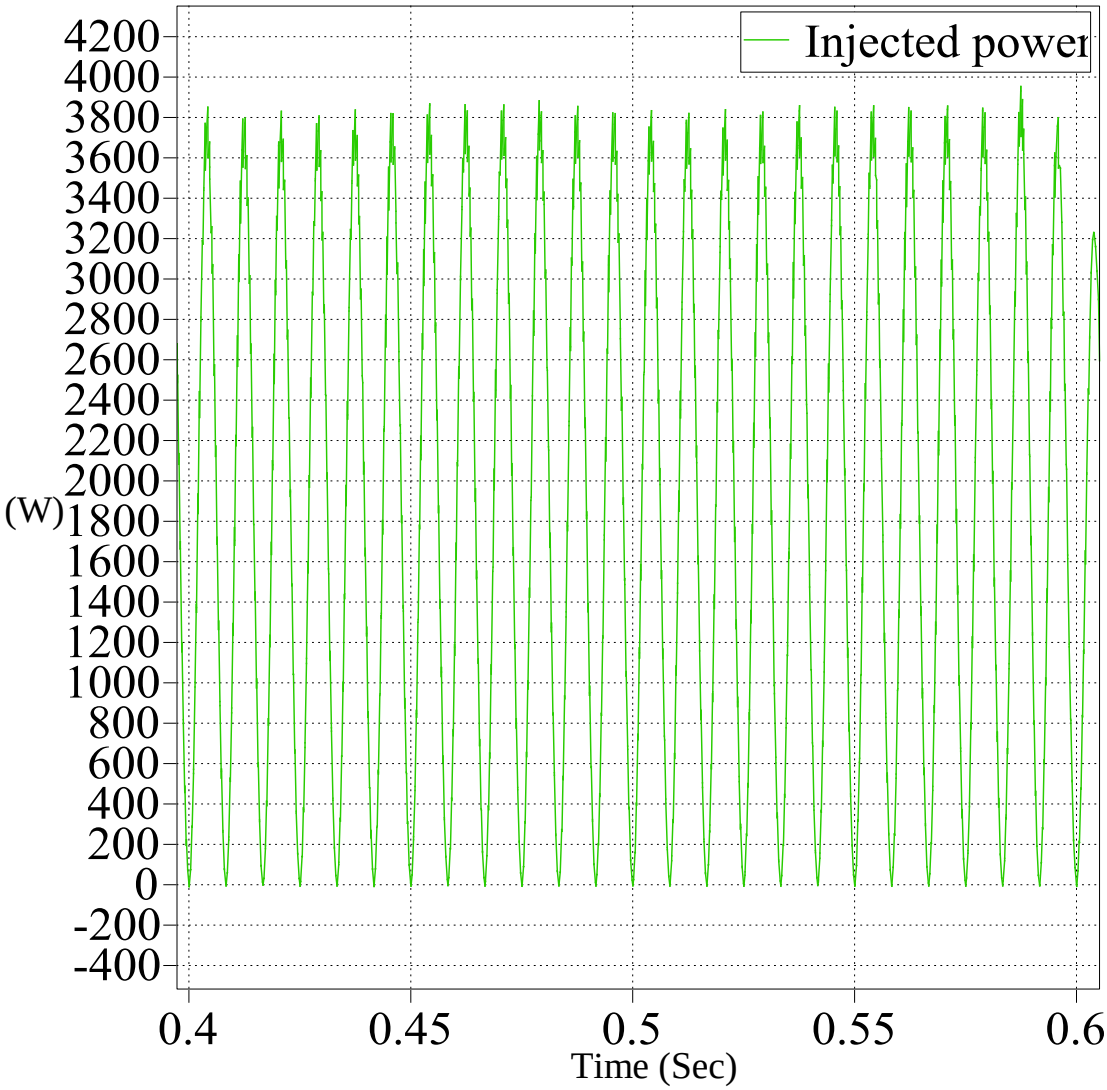

Fig. 7.16: Average power of 1910W being injected into the grid for true MPP.

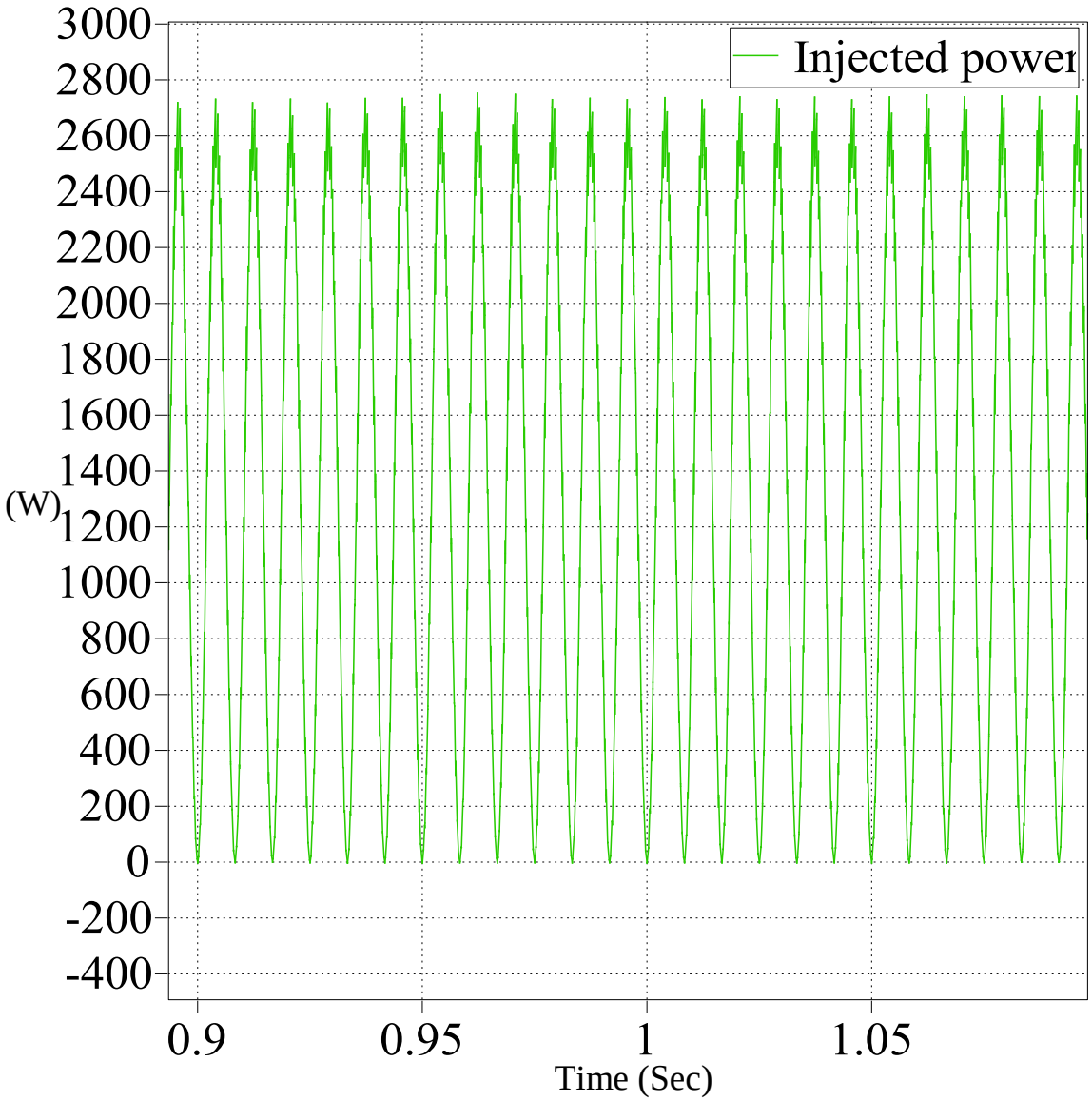

Fig. 7.17: Average power of 1330W being injected into the grid for pseudo MPP.

Figures 7.18 and 7.19 show the zoomed graphs of the active power curves for both the modes of operation of the power plant.

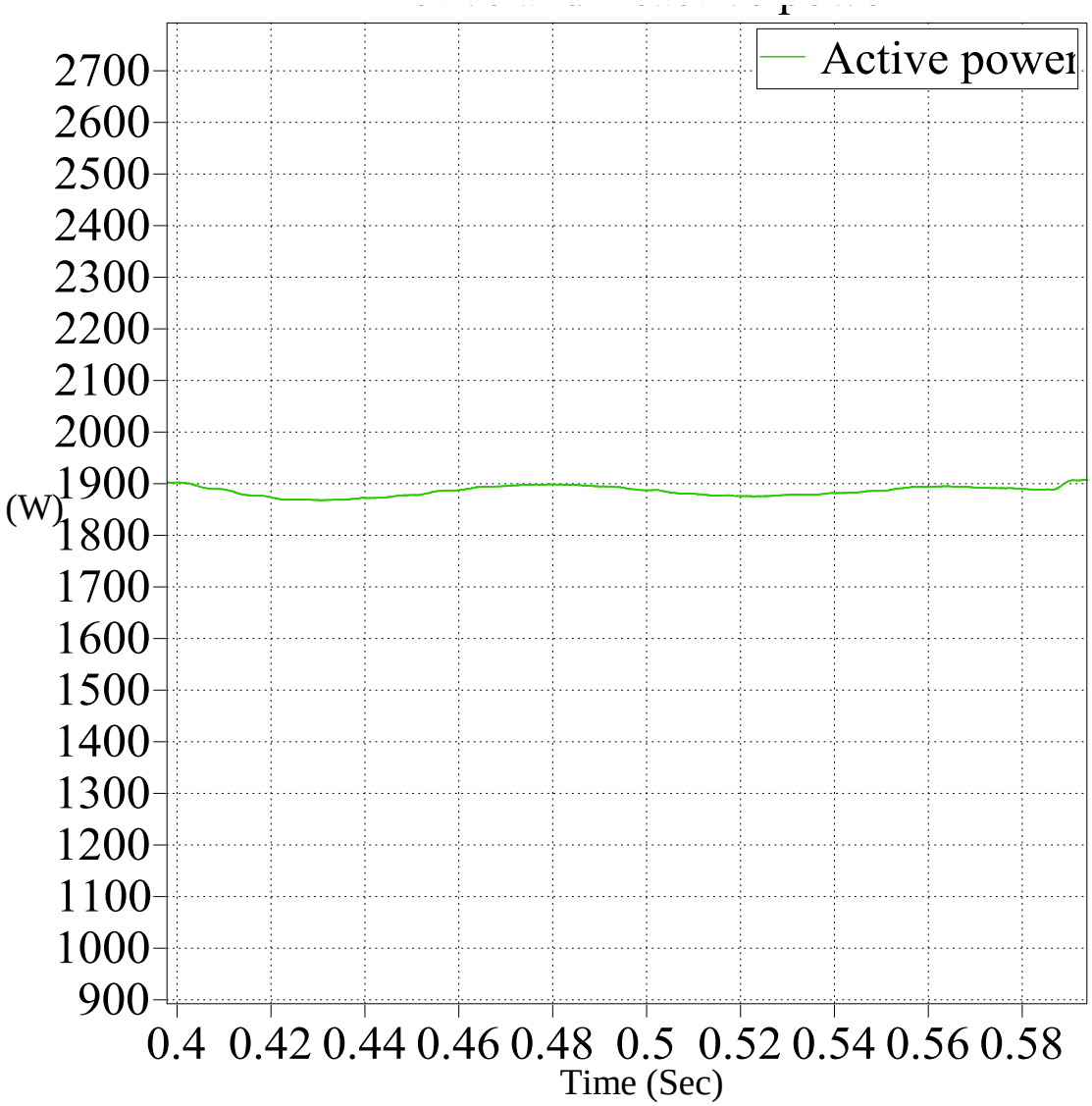

Fig. 7.18: Active power curve for true maximum power at 1000 W/m^2.

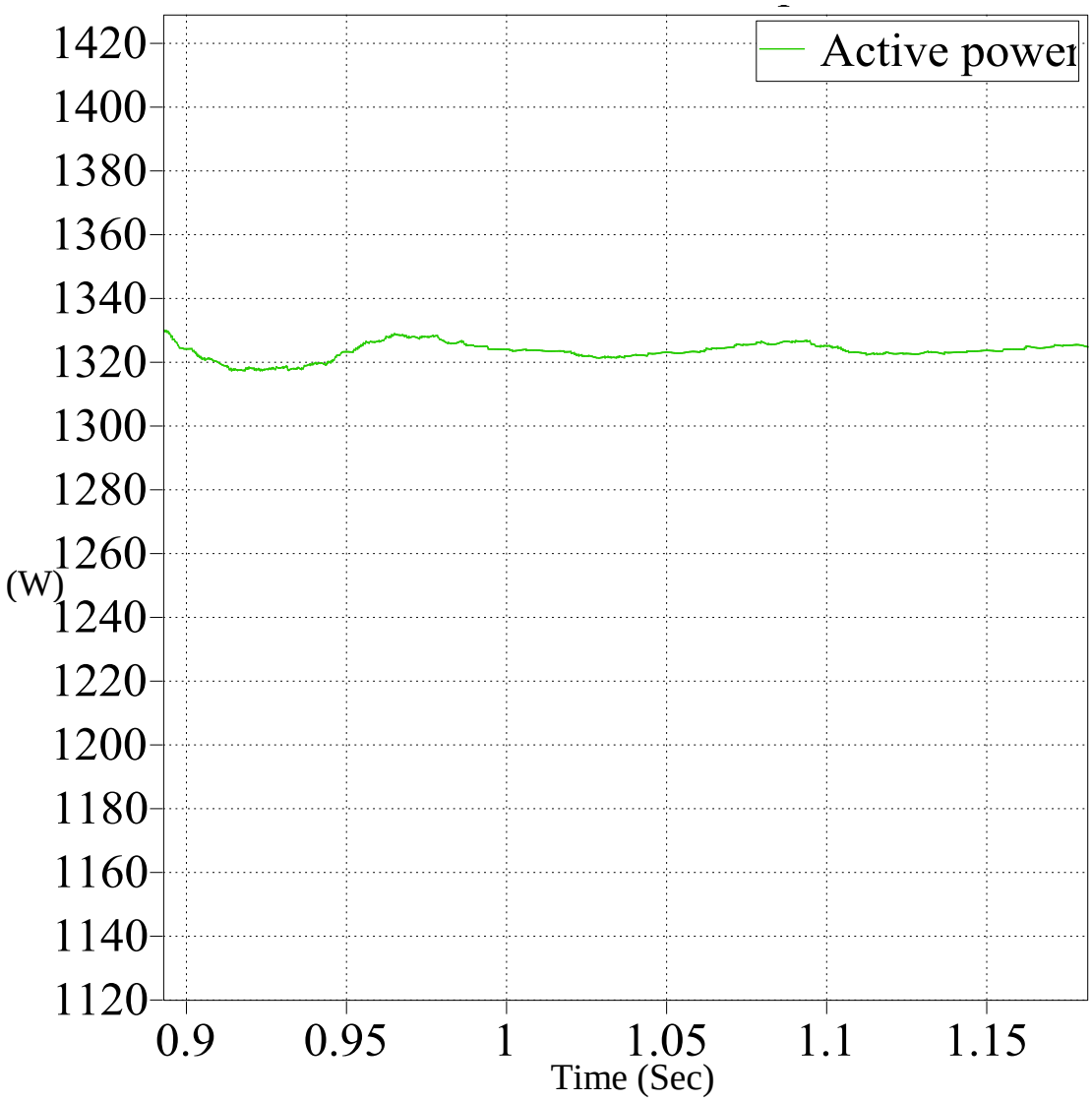

Fig. 7.19: Active power curve for pseudo maximum power at 1000 W/m^2.

Variation in the power at different isolation levels has been discussed in Sections 7.2.1 and 7.2.2. Both cases have reserve power implemented by the PV system. Table 7.1 shows the different values of reserve power that the plant can provide at various insolation levels for a temperature of 25^{o}C.

Table 7.1. Reserve power values for various insolation levels at 25^{o}C

INSOLATION (W/m^2)	TRUE MAX POWER (W)	PSEUDO MAX POWER (W)	RESERVE POWER (W)
1000	1910	800	1110
900	1700	620	1080
800	1490	400	1090
700	1280	225	1055
500	1070	25	1045

An important observation can be made from the results in the first two cases. For a higher temperature of 35^{o}C the amount of reserve power that one gets from the PV plant is less for the same solar irradiance than the case with 25^{o}C. For case B the reserve power is 580W while from Table 7.1 it can be observed that for 25^{o}C the reserve power is 1110W. This is because of change in the voltage tracked by the pseudo power point algorithm at different temperatures.

7.2.3 Case C. This Section checks the operation of the system under uniformly varying insolation at a temperature of 25^{o}C. The varying power on the input and the grid side are shown. Insolation data is shown over a period of 1 sec in Table 7.2. The values shown are the irradiance levels at that particular instant of time. It rises uniformly until 0.5 sec and then falls uniformly until 1 sec of simulation time. To check the performance of the system at a different point on the P-V curve the value of k in the fractional V_{oc} algorithm used is 0.9 for Cases C, D and E.

Table 7.2 Uniformly varying insolation

Time(s)	0	0.1	0.2	0.3	0.4	0.5	0.6	0.7	0.8	0.9	1
Insolation(W/m^2)	200	400	500	600	700	1000	700	600	500	400	200

Figures 7.20 and 7.21 show the variation in the power output from the system when there is a uniform rise and fall of the insolation level incident on the array. For a very short duration at the start of the simulation, the power level is zero, during this time the MPPT takes some time to track the power and reach the operating point.

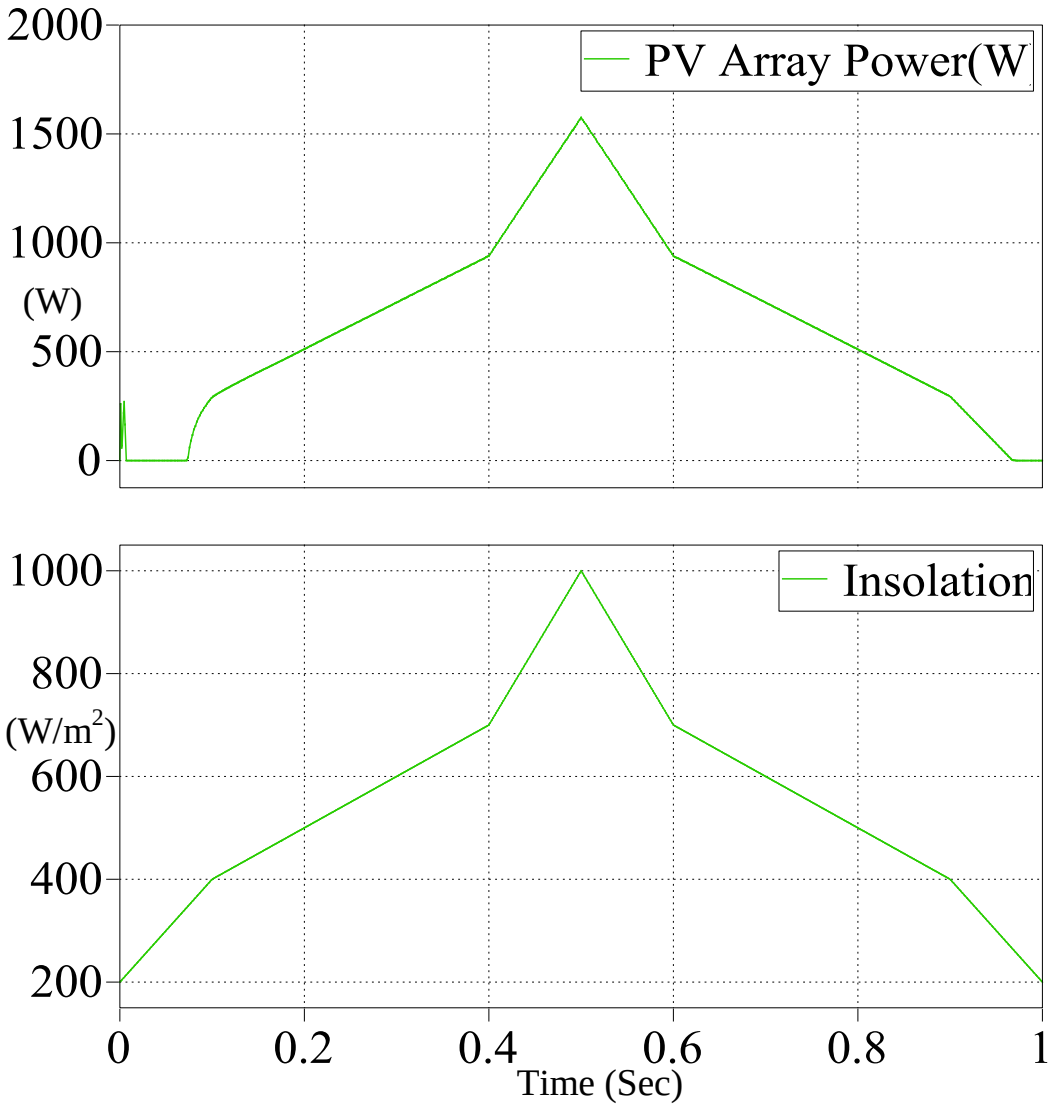

Fig. 7.20: PV output power under uniformly varying insolation for pseudo MPP.

The second curve in the graphs above represents the variation in the insolation with time.

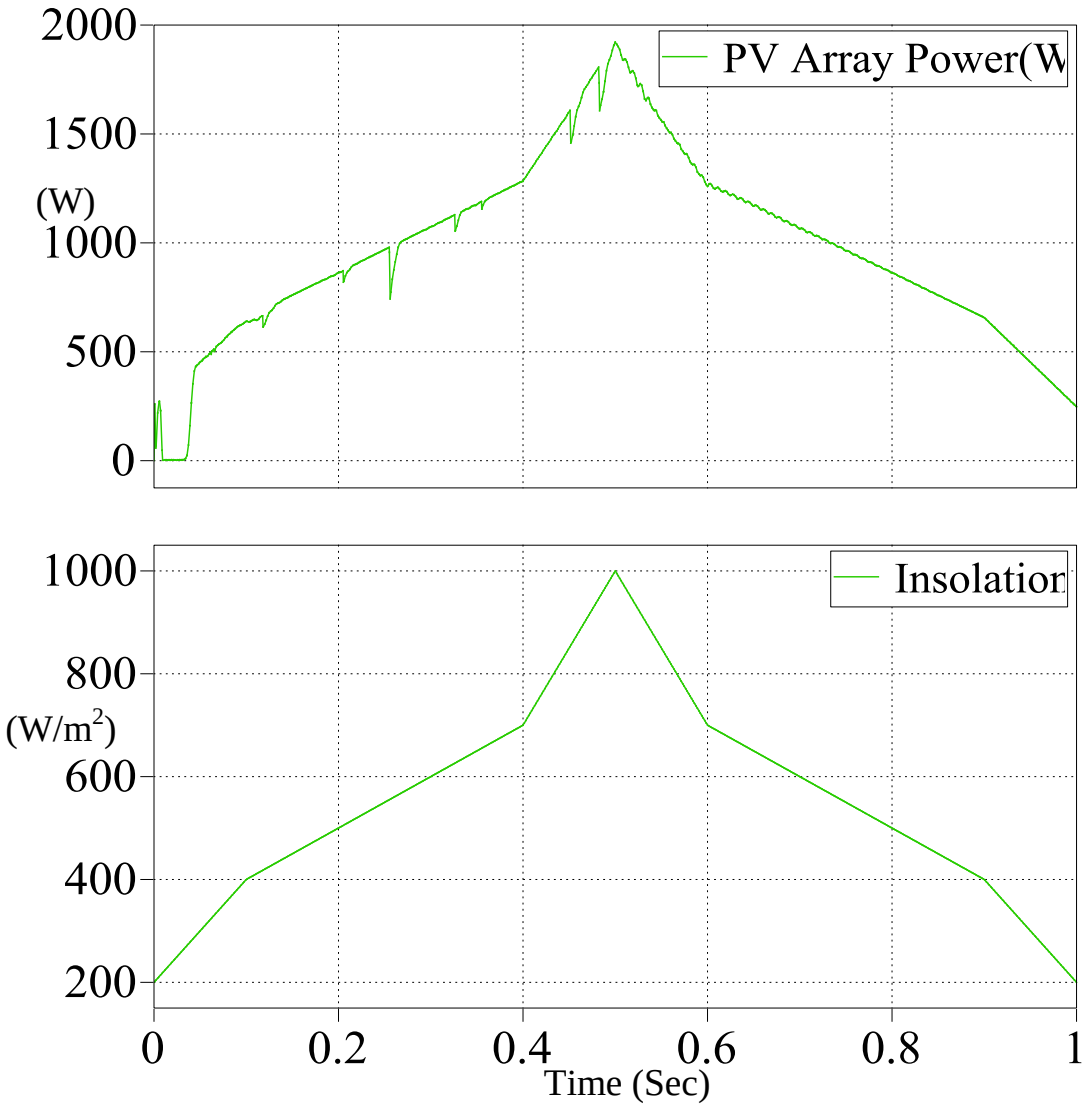

Fig. 7.21: PV output power under uniformly varying insolation for true MPP.

Figures 7.22 and 7.23 are the active power curves for varying insolation under pseudo and true power modes, respectively.

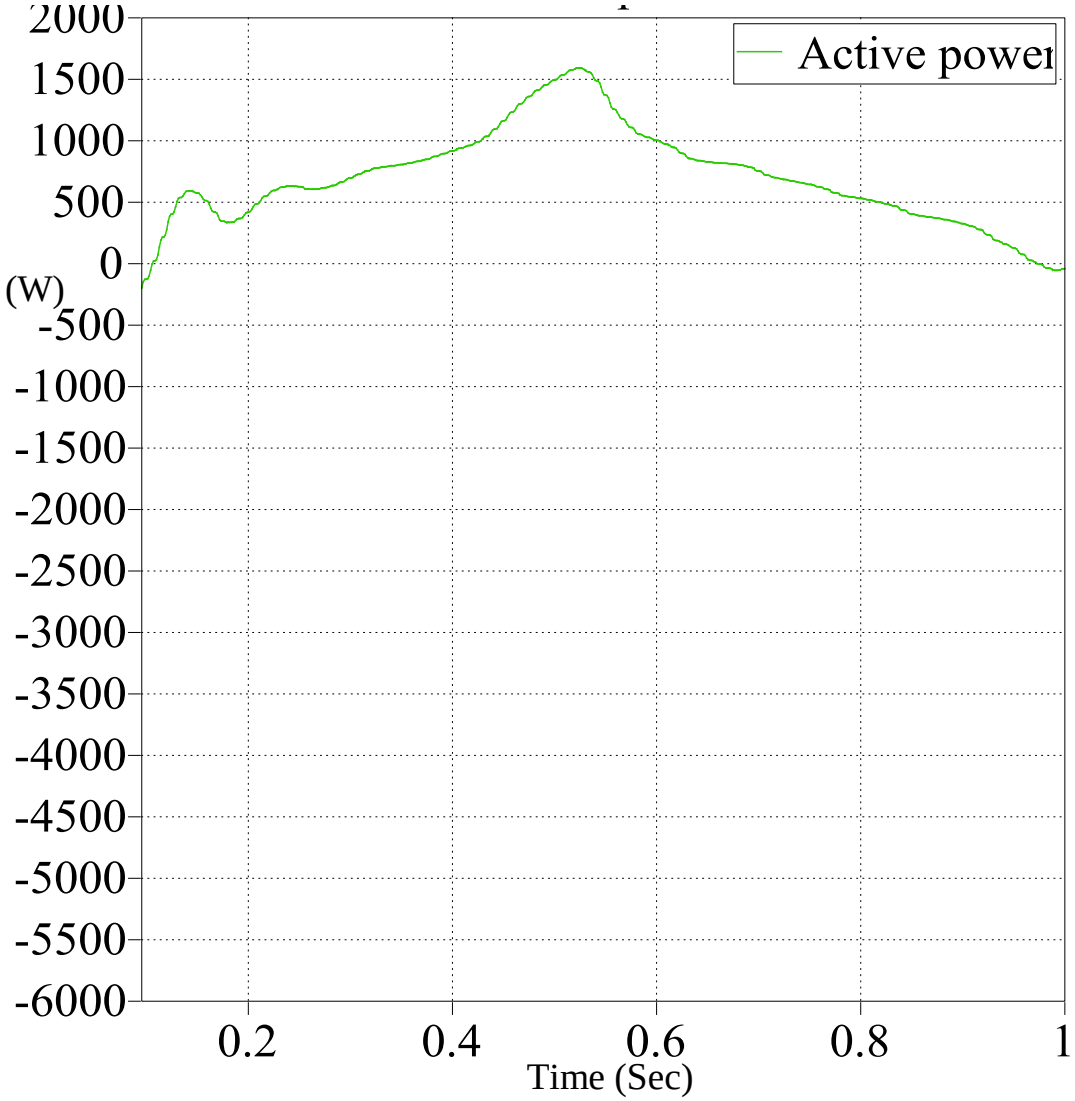

Fig. 7.22: Active power curve for varying insolation (Pseudo MPP).

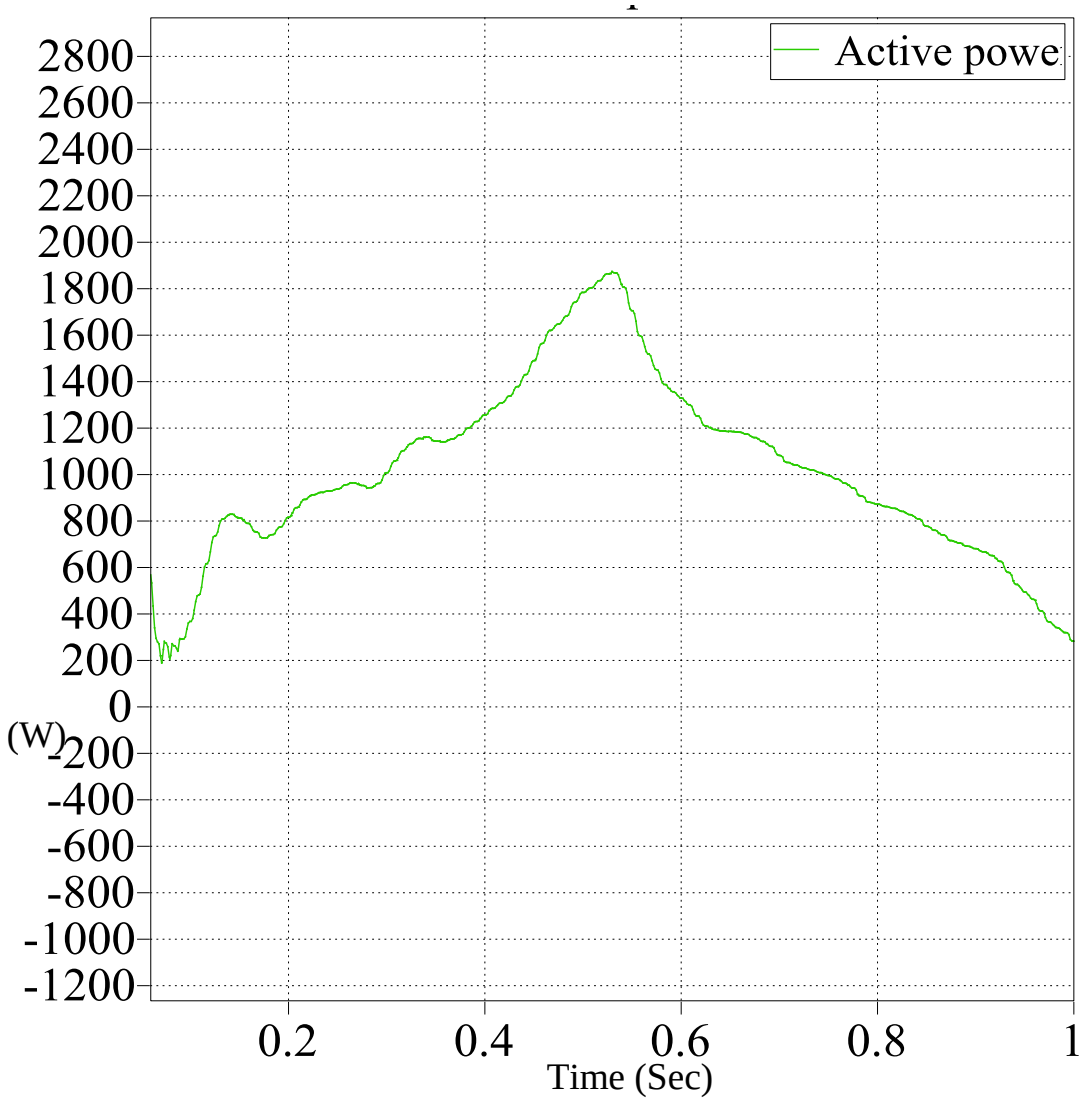

Fig. 7.23: Active power curve for varying insolation (True MPP).

Figure 7.21 is the power generated in the PV system, while Figs. 7.22 and 7.23 show the same amount of power being injected into the grid for both power modes.

7.2.4 Case D. This case checks the system output for non-uniform insolation incident on the PV array at a temperature of 25^{o}C. Insolation data is shown in Table 7.3.

Table 7.3 Non-uniformly varying insolation

Time(s)	0	0.1	0.2	0.3	0.4	0.5	0.6	0.7	0.8	0.9	1
Insolation(W/m^2)	200	450	650	600	400	700	900	550	850	620	450

Figure 7.24 shows the variation in output power for pseudo MPP and Fig. 7.25 shows the variation in output power under true MPP. In both cases for a short period of time, the power is zero since during this time; the MPP is trying to track the power point on the curve.

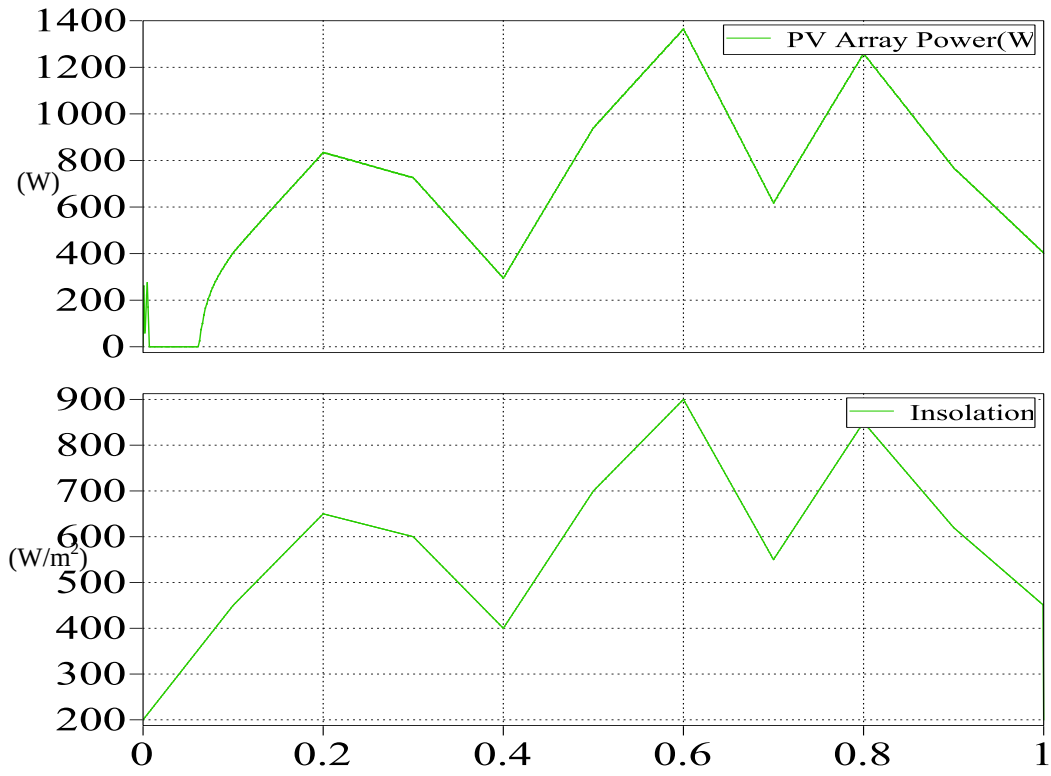

Fig. 7.24: PV output under non-uniform insolation (Pseudo MPP).

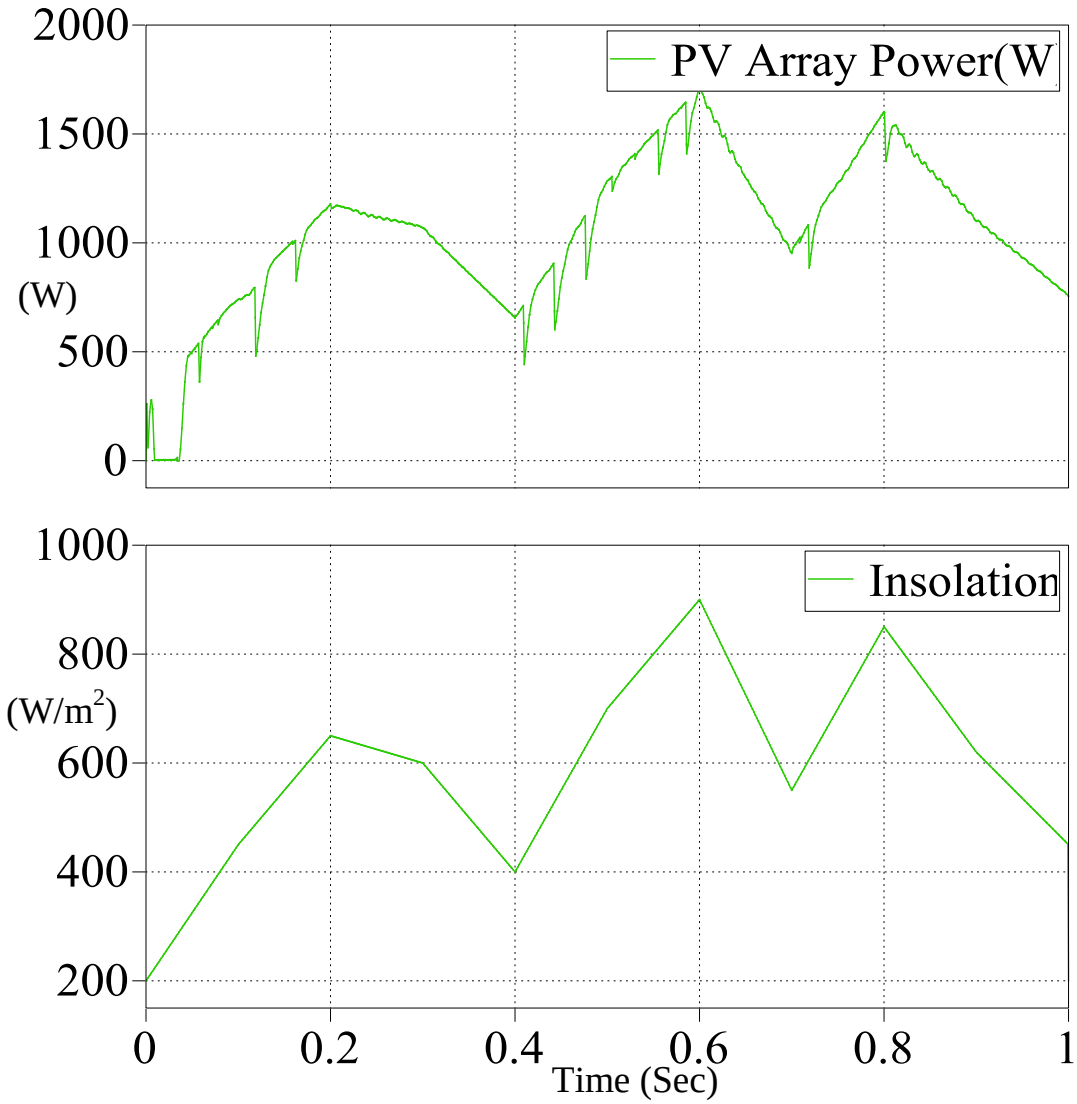

Fig. 7.25: PV output under non-uniform insolation (True MPP).

Figures 7.26 and 7.27 show the active power curves under pseudo and true power points, respectively for non-uniformly varying insolation.

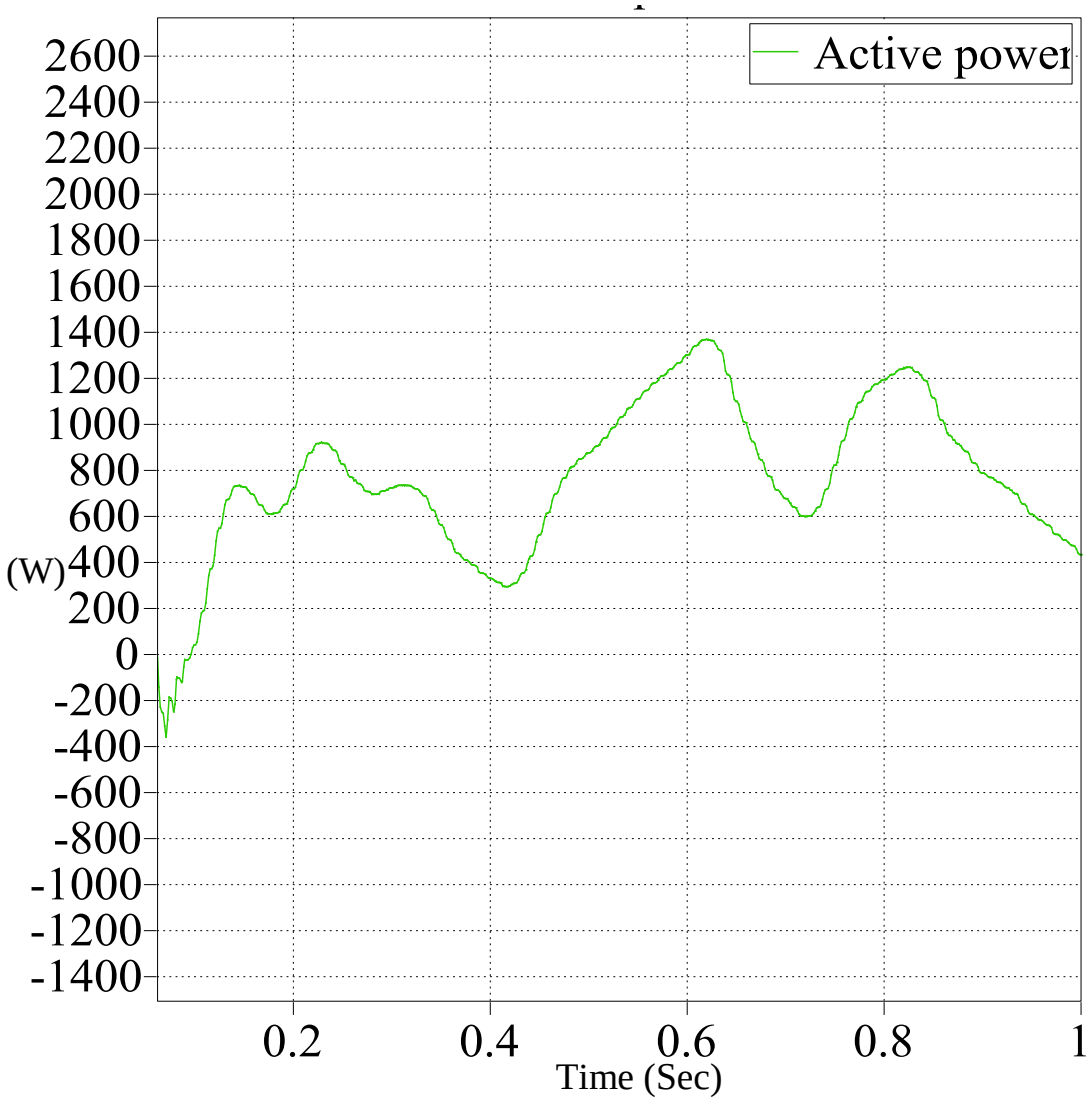

Fig. 7.26: Active power curve for non-uniform insolation (Pseudo MPP).

Figures 7.24 and 7.25 show the power generated in the PV system at the source side while Figs. 7.26 and 7.27 show the same amount of power being injected into the grid side.

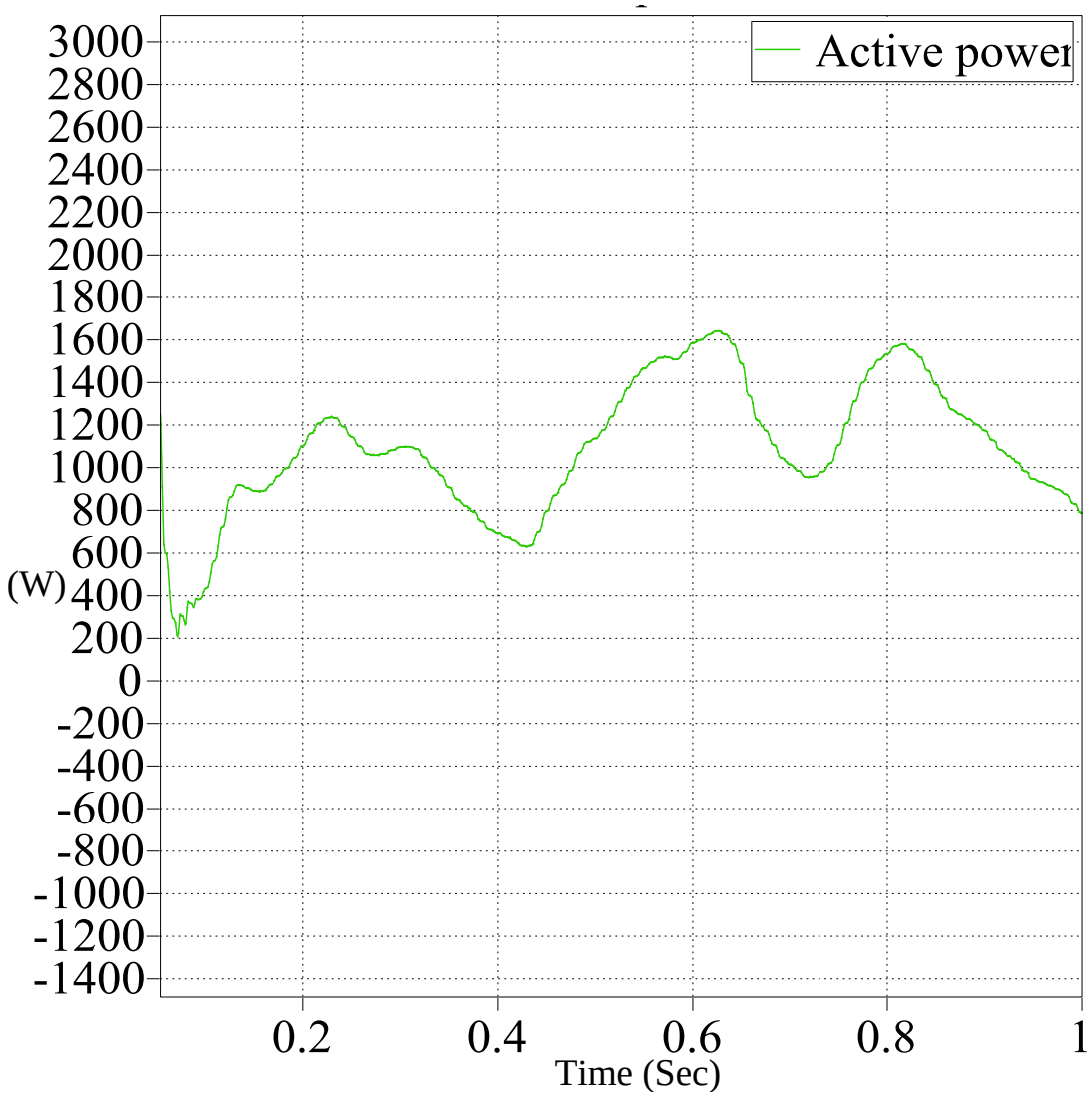

Fig. 7.27: Active power curve for non-uniform insolation (True MPP).

7.2.5. Case E. This Section tests the system for injecting active and reactive power into the grid at a power factor of 0.8. The temperature is 25^{o}C and the insolation is 1000W/m^{2}

Figure 7.28 shows the variation in the magnitude of the voltage and current for the two different power modes.

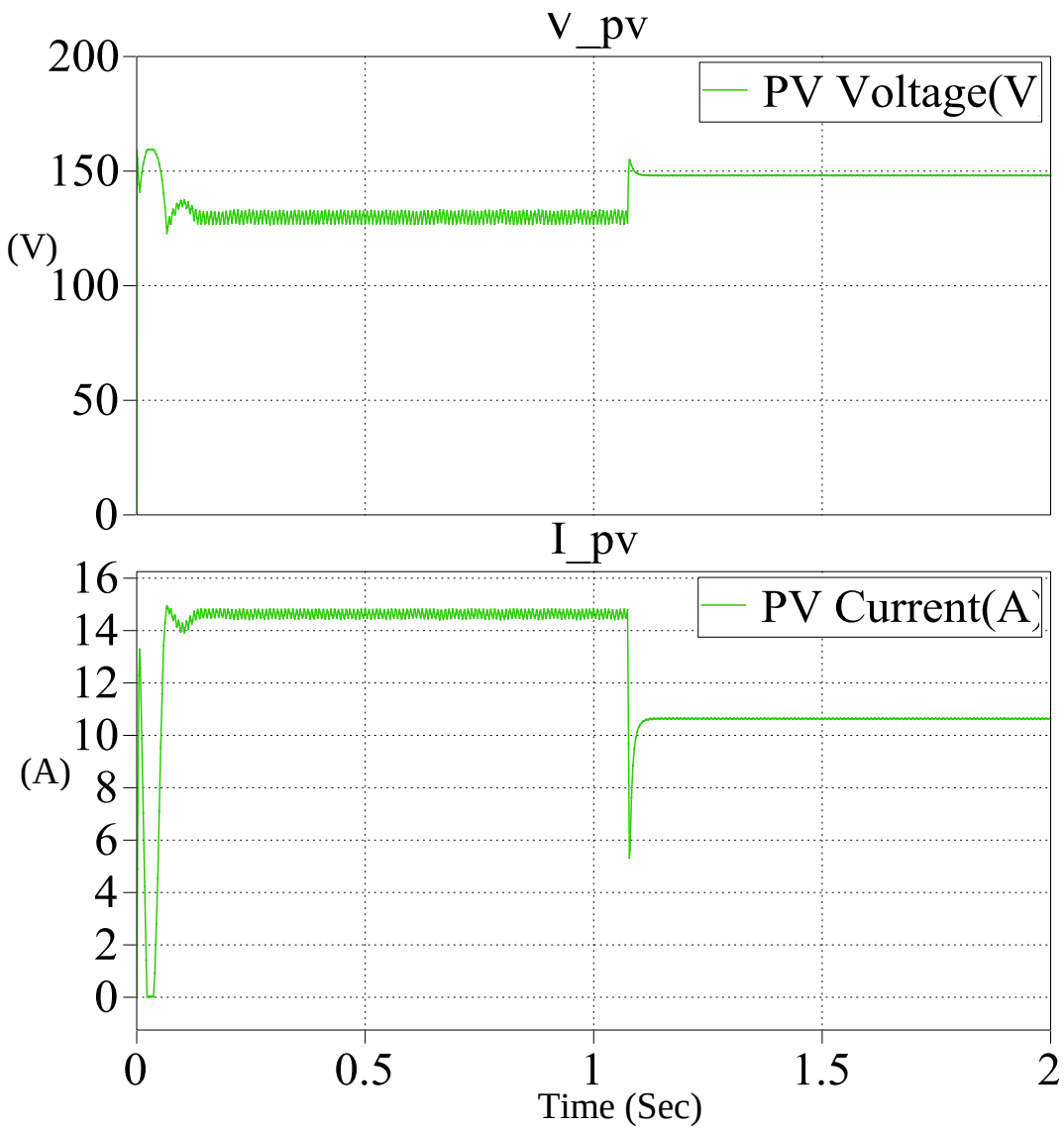

Fig. 7.28: PV voltage and current.

Figures 7.29 and 7.30 show the net power injected at the grid side for true MPP and pseudo MPP, respectively.

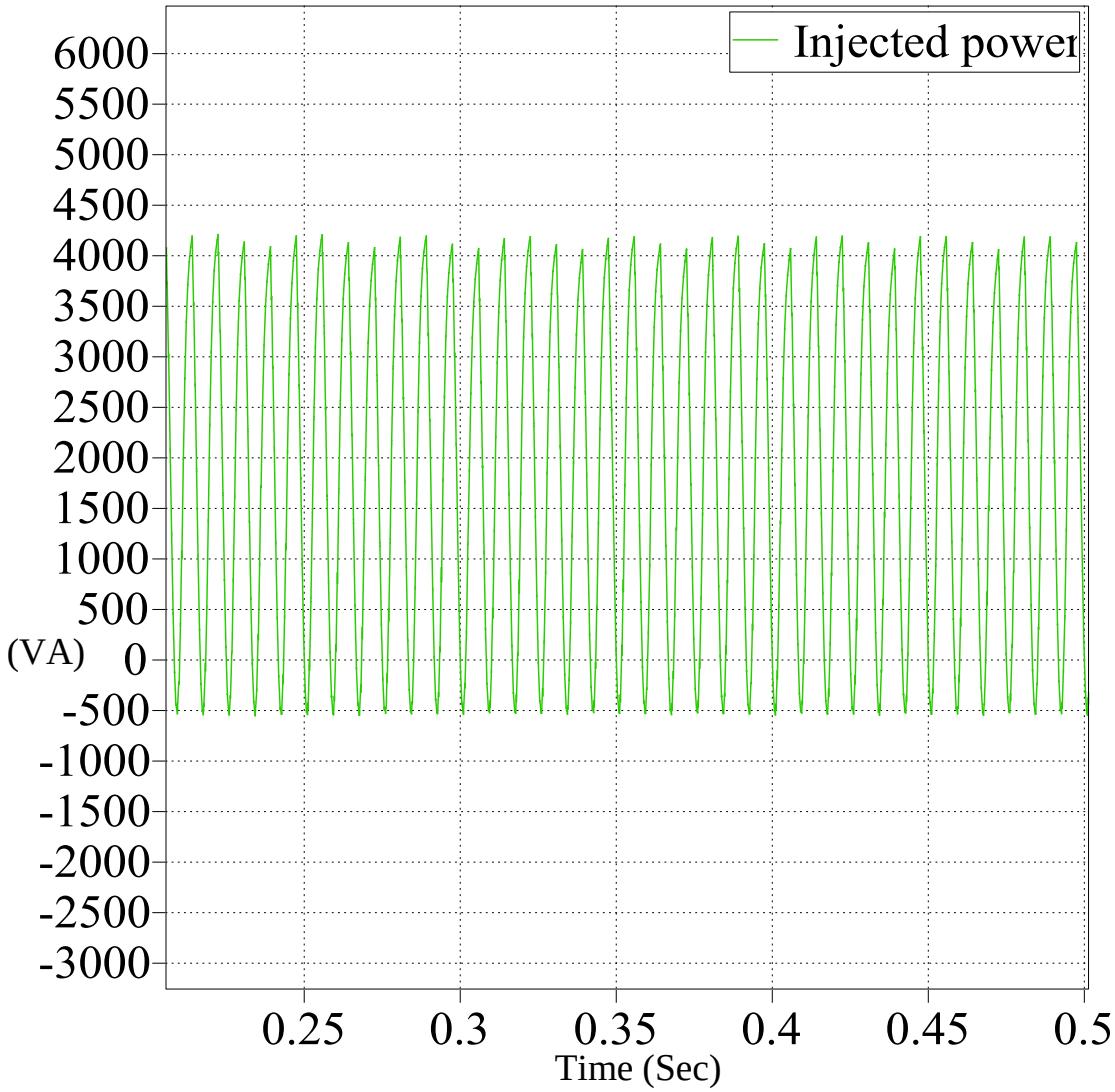

Fig. 7.29: Power at grid side for true MPP.

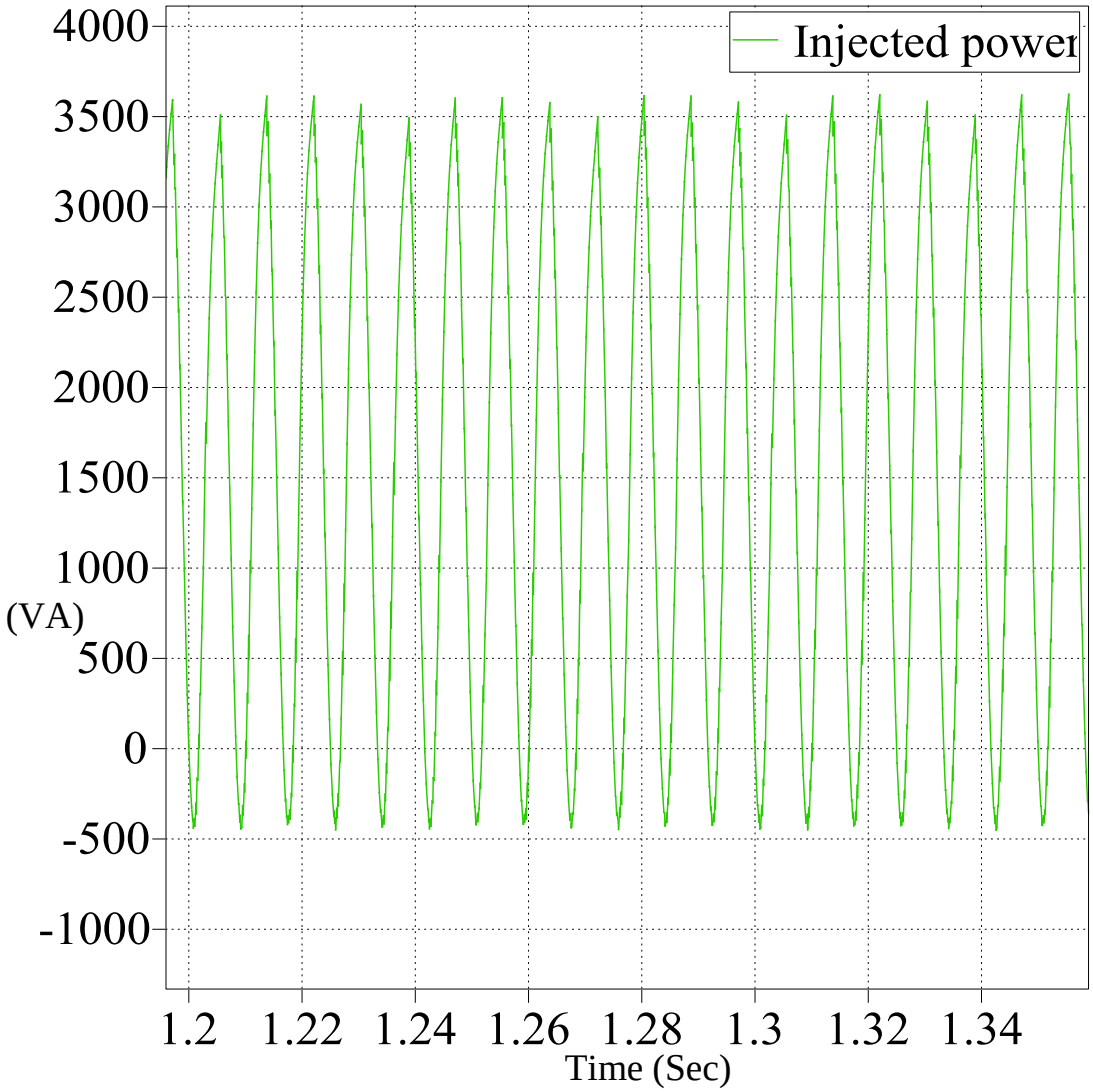

Fig. 7.30: Power at grid side for pseudo MPP.

Figure 7.31 shows the variation in the active and reactive power magnitudes for the low and high power operations at 0.8 power factor. This is injected at a voltage of 340V p-p. It can be observed that the system responds in a fast way to a change in load or frequency in the power grid. This can be effectively used in the implementation of frequency regulation for the system.

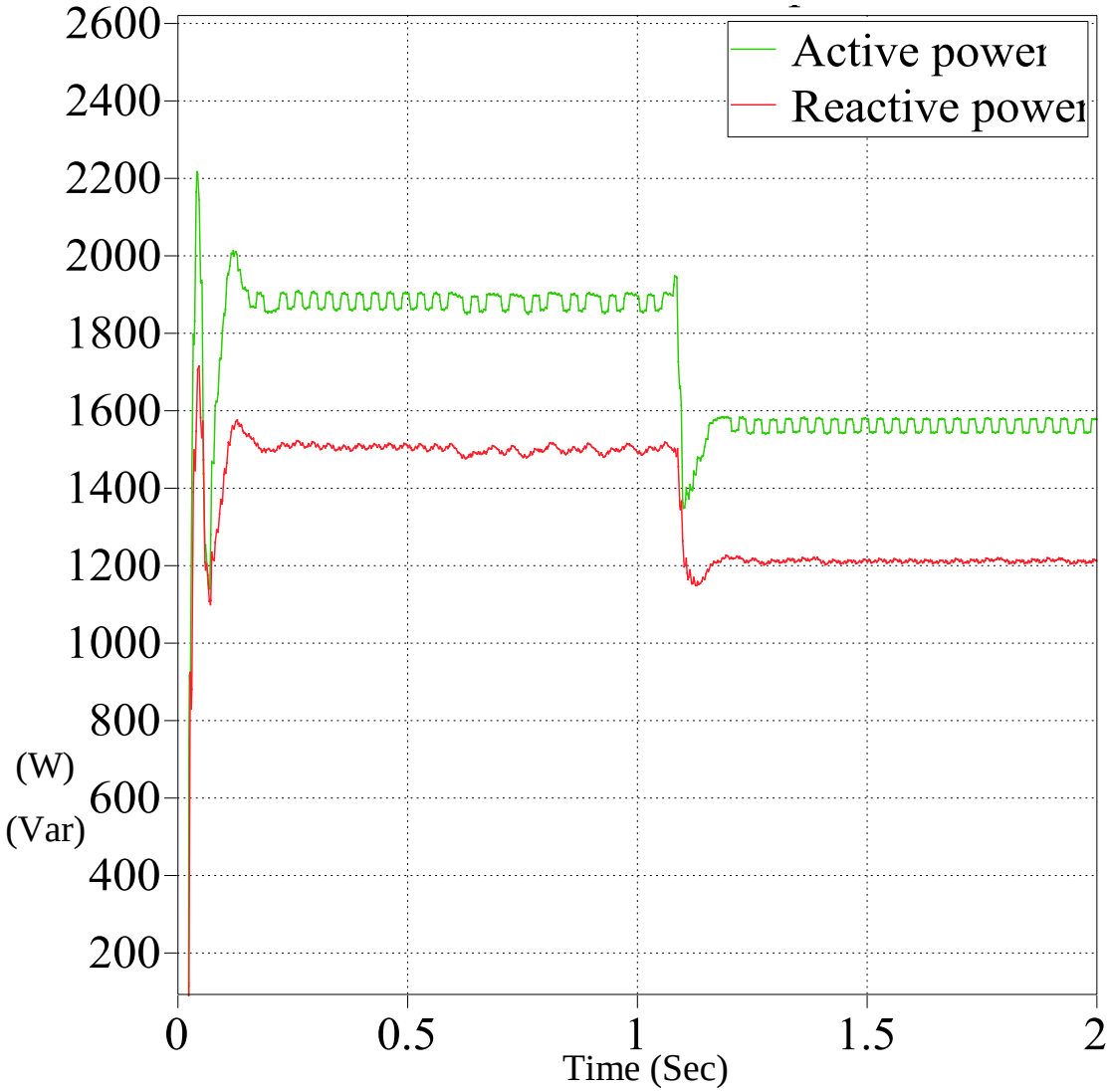

Fig. 7.31: Active and reactive power magnitudes at 0.8 p.f. lag on the grid side.

7.3. RELATION BETWEEN k AND PSEUDO POWER

The system's pseudo power capability with different values of k was observed. Table 7.4 shows the variation in the value of k for the fractional V_{oc} algorithm as explained in Fig. 5.5 in Section 5. Figure 7.32 shows the pseudo power variation as a function of k when the temperature is held constant at 25^{o}C and irradiance is 1000 W/m^{2}.

Table 7.4 Relation between k and pseudo power

K	Pseudo power
0.3	870
0.4	1000
0.5	1260
0.6	1500
0.7	1740
0.85	1865
0.9	1500
0.92	1200
0.94	700
0.95	400

The maximum amount of reserve power from the system can be achieved for either very low values of k (left side of P-V curve) or high values of k (right side of P-V curve). The reserve power margin is very low for values of k close to the maximum power point (k=0.85). It can be observed from Fig. 7.32 that the relation between k and pseudo power is non linear.

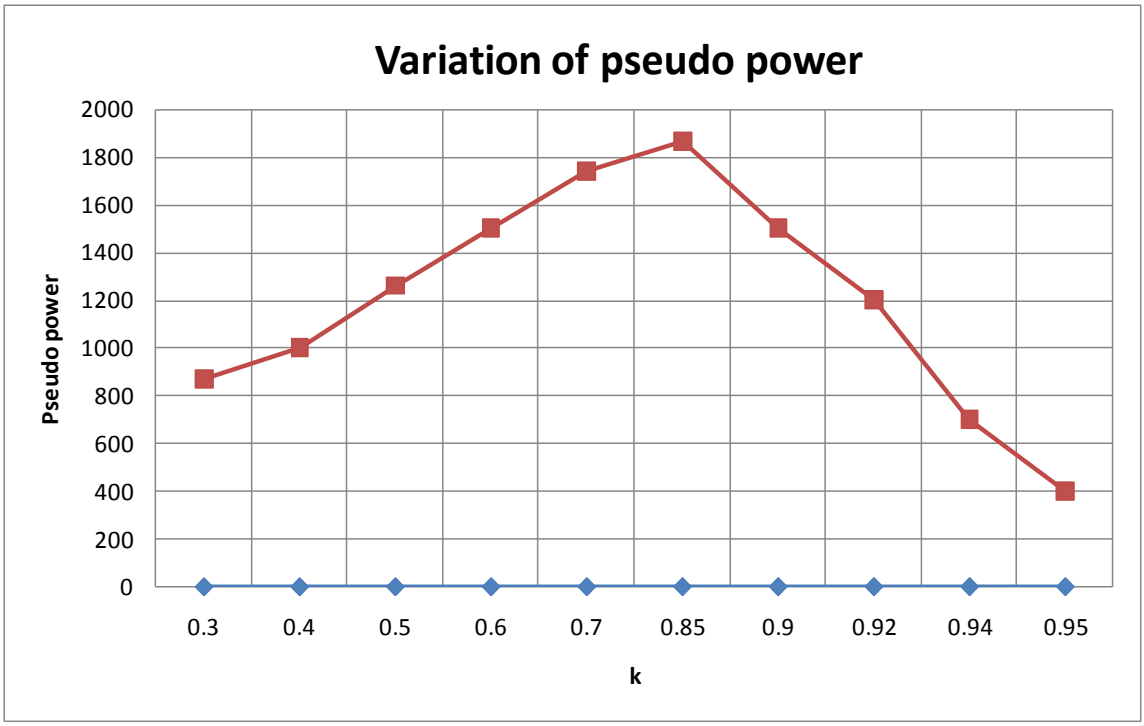

Fig. 7.32: Variation of pseudo power point with change in value of k.

8. CONCLUSION AND FUTURE WORK

8.1. CONCLUSION

The PV technology, although promising in many aspects, suffers from several drawbacks such as relatively higher cost, low efficiencies, inherent output intermittency and daily availability that could be lower than 50%. Yet, it is one of the more mature, easily available renewable energy technologies that are currently being used for utility-scale generation. Control of power from the PV plant under such generation scenarios becomes essential to enable it to participate in grid operation procedures. The frequency regulation capability for the PV plant has been proposed for possible use in load following schemes, particularly in microgrid application. This method allows for effective control of solar power for various purposes without compromising the efficiency of conversion.

Simulation studies have been done to test the system under constant and varying insolation cases and also at different temperatures. The frequency regulation capability has been simulated by using control over the MPPT algorithm based on the external frequency signal of the grid, which conveys the need for active power. The studies reported in this thesis have shown that the response of the PV plant to changes in power demand is instantaneous under different cases.

The amount of reserve power available from a PV plant for a given irradiance is dependent on the temperature. The higher the temperature, the lower is the reserve power available for control and vice versa. It was proven by simulation that the PV system is capable of providing power at a power factor other than unity, if called upon.

The simulation of the solar array and the MPPT were designed as mathematical models in Simulink, while the power conversion stage was designed on PLECS platform as real time circuits. This had been done to accommodate the solar cell's behavior as a mathematical equation which is not possible in PLECS. The same procedure is adopted with the MPPT and inverter control blocks because they use logical reasoning and programming to send control signals for switching the semiconductor devices.

Applying the reserve power technique to the PV system under various conditions enabled it to behave as a conventional generation source which can vary its power output with respect to the system's need. Since there are two possible points for the same reserve power on the P-V curve any of these two can be used to achieve the objective. But, the right side of the curve was used to reduce the ripple voltage in the boost converter output.

The reserve power technique is very useful for fast temporary response actions, and not for long term load control. The time of reserve power availability depends on the time of day and weather conditions. Implementation of the reserve margin on a longer term basis should be done with assist from an energy storage device or a stand-by generator.

8.2. FUTURE WORK

This thesis has shown a new methodology to make solar PV plants more reliable for participating in power system operations and control. Future work can be extended to make this system work along with an energy storage, most likely in the form of battery storage, to help in long term control and also during intermittent PV output variations. The variation in the value of ‘k’ in the fractional Voc algorithm plays a key role in the implementation of reserve power in the system. This can be extended to make the value of ‘k’ dynamic so that it changes with time based on the amount of reserve power needed by the grid.

APPENDIX A.
ONLINE SEARCH ALGORITHM

```
% Maximum power tracking using online search algorithm
function y = del(u)        % Call function for Vref
global del;
global Im;
global Pm;
global Vm;
Ptol=0.001;          % Tolerance value for power difference
Pop=(u(1)*u(2));      % Operating value for Power
delVmax=2;           %Maximum limit on the change in reference voltage
delVmin=-2;          %Minimum limit on the change in reference voltage
X=del;
E=0;
if (Pop-Pm) < Ptol
   del=X;
elseif (u(2)-Im)==0&&(u(1)-Vm)==0
    del=X;
else
    E=(u(1)*((u(2)-Im)/(u(1)-Vm)))+u(2); % Error in the value dP/dV
end
delV=0.1*E;              %Change in the reference voltage
if del>delVmax           % Imposing limits on delV change
    del=delVmax;
elseif del<delVmin
```

```
    del=delVmin;
end
del=del+delV;
Pm = Pop; Vm=u(1);Im=u(2);  % Update the Pm, Vm and Im variables
y=del;                      % Change in reference voltage
```

APPENDIX B.
MODIFIED FRACTIONAL OPEN CIRCUIT VOLTAGE ALGORITHM

```
% Pseudo Maximum power tracking using modified Fractional Voc Method
function y = del1(u)
global del1;
global Ia1;
global Pa1;
global Va1;
T=25;       % Operating temperature of the array
Pop1=(u(1)*u(2));
delVmax1=40;%Maximum limit on the change in reference voltage
delVmin1=-40;%Minimum limit on the change in reference voltage
X1=del1;
% Temperature dependent equation V_oc' = [V_oc + (K_v × (T − 25))]
Voc=164.5+5*(-0.12*(T-25));% Open circuit voltage
E1=0;
if (u(1)==(0.5*Voc))&&(Pop1-Pa1)>0
  del1=X1;
else
   E1=(0.5*Voc)-u(1); % Error in the voltage
end
delV1=0.1*E1;
if del1>delVmax1       % Imposing limits on del1
   del1=delVmax1;
elseif del1<delVmin1
```

```
    del1=delVmin1;
end
del1=del1+delV1;
Pa1 = Pop1; Va1=u(1);Ia1=u(2);
y=del1;              % Change in reference voltage
```

APPENDIX C.
INVERTER SWITCHING ALGORITHM

```
if (GridAngle >= 0)    % Checks for the sign of grid angle
   if (dI >= 0)        % Difference in the reference value of grid current and the
                       %reference current
      VectorSelect = 2;
   else
      VectorSelect = 0;
   end
else
  if (dI >= 0)
     VectorSelect = 0;
   else
      VectorSelect = 3;
   end
end
```

BIBLIOGRAPHY

[1] http://www.ases.org/images/stories/file/ASES/climate_change.pdf Jan 2010.

[2] http://www.pvresources.com/en/top50pv.php Jan 2010.

[3] K.D. Brabandere, K. Vanthournout, D.J. Deconinck, G.R. Belmans, 2007, "Control of Microgrids," IEEE Power Engineering Society General Meeting, pp. 1 – 7. 2007.

[4] F. Katiraei, R. Iravani, N. Hatziargyriou, A. Dimeas, "Microgrid management: control and operation aspects of Microgrids," IEEE Power and Energy Magazine, vol. 6, pp. 54-65, May/June 2008.

[5] B. Kroposki, R. Lasseter, T. Ise, S. Morozumi, S. Papathanassiou, N.Hatziargyriou, "Making microgrids work," IEEE Power and Energy Magazine, vol. 6, pp 41-53, May/June 2008.

[6] N. Jayawarna, X. Wu, Y. Zhang, N. Jenkins, M. Barnes, "Stability of a MicroGrid," The 3rd IET International Conference on Power Electronics, Machines and Drives, pp. 316 – 320, Mar 2006.

[7] Y. Chen, K.M. Smedley, "A cost effective single stage inverter with maximum power point tracking," IEEE Transactions on Power Electronics, vol. 19 , pp. 1289 – 1294, Sept 2004.

[8] R. Gules, P.D. Pellegrin, J. Hey, H.L.J. Imhoff, "A Maximum Power Point Tracking System with Parallel Connection for PV Stand-Alone Applications," IEEE Transactions on Industrial Electronics, vol. 55, pp.2674 – 2683, July 2008.

[9] H. Liao, C. Xu, J. Song ,Y. Yu, "Green Power Generation Technology for Distributed Power Supply," International Conference on Electricity Distribution, pp. 1-4, Dec 2008.

[10] http://www.solarbotics.net Jan 2010.

[11] http://www.solar-power-answers.co.uk/ Jan 2010.

[12] C.L. Jeong; W.J. Sang; Y.H. Jae; K.K. Seok, S. Jinsoo; Y.H. Kyung; "Si-based thin-film solar cells: process and device performance analysis," Photovoltaic Specialists Conference, Conference Record of the Thirty-first IEEE pp. 1552 – 1555, Jan. 2005.

[13] R. Hezel; C. Schmiga, A. Metz, "Next generation of industrial silicon solar cells with efficiencies above 20%," IEEE Conference Record of the Twenty-Eighth Photovoltaic Specialists Conference, pp.184 – 187, Sept. 2000.

[14] T. Yuki, H. Yoshihiro, K. Kosuke, "Temperature and Irradiance Dependence of the I-V Curves of Various Kinds of Solar Cells," 15th International Photovoltaic Science & Engineering Conference (PVSEC-15), National Institute of Advanced Industrial Science and Technology (AIST), Research Center for Photovoltaics, Japan, 2005.

[15] A. Yazdani, "General Guidelines for Modeling, Control Design, and Simulation of Single-Stage Grid-Connected PhotoVoltaic (PV) Systems."

[16] I Serban,.; C.P Ion,.; C Marinescu,.; M Georgescu, "Frequency Control and Unbalances Compensation in Autonomous Micro-Grids Supplied by RES," IEEE International Electric Machines & Drives Conference, vol. 1, pp. 459 – 464, May 2007.

[17] S.Wijnbergen, S.W.H. de Haan, J.G. Slootweg, "A System for Dispersed Generator Participation in Voltage Control and Primary Frequency Control of the grid," 36th IEEE Power Electronics Specialists Conference, pp. 2918 – 2924, June 2005.

[18] G.R Walker, "Evaluating MPPT converter topologies using a Matlab PV model," Journal of Electrical & Electronics Engineering, Australia, vol. 21, 2001.

[19] I.M. Frederick, N.E. Lars, "Design and implementation of a digitally controlled stand alone PV supply," Nordic Workshop on Power and Industrial Electronics, Aug 2002.

[20] http://ecee.colorado.edu/~ecen2060/energyprogram.html Dec 2008.

[21] I.H Altas, A.M Sharaf, "A Photovoltaic Array Simulation Model for Matlab-Simulink GUI Environment," International Conference on Electrical Power, pp. 341 – 345, May 2007.

[22] M. Francisco L. González, "Model of Photovoltaic Module in Matlab," Latin American Congress of Students of Electrical Engineering, Electronic and Computation, 2005.

[23] R.Ito, Y Matsuzaki, T. Tani,; T Yachi, "Evaluation of performance of MPPT equipment in photovoltaic system," The 25th International Telecommunications Energy Conference, pp. 256 – 260, Oct 2003.

[24] T. Esram, P.L. Chapman, "Comparison of Photovoltaic Array Maximum power Point Tracking Techniques," IEEE Transactions on Energy Conversion, Vol 22, pp. 439 – 449, June 2007.

[25] K.A. EL-Serafi, A.E. Kalas, M. H. Elfar, "On-Line Maximum Power Tracking In a Stand Alone Photovoltaic System," Suez Canal University, Faculty of Engineering, 2003.

[26] R.W. Erickson, *"Fundamentals of Power Electronics,* Second Edition, Secaucus, NJ, USA. Kluwer Academic Publishers, 2000.

[27] V. Tipsuwanporn, C. Sodaban, P. Thepsatorn, "Adaptive Switching Frequency in Delta Modulation Inverter for Single Phase Induction Motor Drives," IEEE International Conference on Industrial Technology, pp. 599-603, Dec 2005.

[28] N.A. Ninad, L.A.C. Lopes, 2007, "Operation of Single Phase Grid Connected Inverters with Large DC Bus Voltage Ripple," IEEE Canada Electrical Power Conference, pp. 172 – 176, Oct 2007.

[29] M.E. Ropp, S. Gonzalez, "Development of a MATLAB/Simulink Model of a Single-Phase Grid-Connected Photovoltaic System," IEEE transactions on Energy conversion, vol. 24, pp. 195-202, Mar 2009.

[30] M. Ciobotaru, T. Kerekes, R. Teodorescu, A. Bouscayrol, "PV inverter simulation using MATLAB/Simulink graphical environment and PLECS blockset," 32nd Annual IEEE Conference on Industrial Electronics, pp. 5313 – 5318, Nov 2006.

[31] X. Jinhui, Y. Zhongdong, S. Qipeng, S.Renzhong, "Analyze and research of the inverter for grid-connecting photovoltaic system," Third International Conference on Electric Utility Deregulation and Restructuring and Power Technologies, pp. 2530 – 2535, April 2008.

VITA

Venkata Ajay Kumar Pappu was born on July 9, 1985, in Ongole, India. He obtained his Bachelor's degree in Electrical and Electronics Engineering from Vellore Institute of Technology University, Vellore, India in May 2008. He joined Missouri University of Science and Technology (formerly University of Missouri - Rolla) in the Fall of 2008 for his Masters degree in Electrical Engineering. He received his Masters degree in Electrical Engineering in December 2010 from the Missouri University of Science and Technology, Rolla, Missouri. He had a summer internship at the California Independent System Operator, Folsom, CA in the summer of 2009.